



Measurement of effective diffusion coefficients of porous fuel cell electrodes

Rinat Rashapov

Department of Chemical Engineering

McGill University

Montreal, Quebec

December 2014

A thesis submitted to McGill University in partial fulfillment of the requirements of the degree of Master of Engineering

© Rinat Rashapov, 2014

Abstract

A new experimental technique for measuring the in-plane components of the effective diffusivity tensor of thin porous materials is presented. The method is based on the transient diffusion of oxygen from air into a porous sample initially purged with nitrogen. The oxygen concentration is measured at a fixed location in the sample with time and the response is fitted to an analytical solution of Fick's law for one-dimensional, transient diffusion. The sample holder was designed to allow varying degrees of compression, thereby changing the porosity and tortuosity of the material. The present method provides accurate, fast, and repeatable measurements, is applicable to electrically conductive materials, uses a simple sample holder, an off-the-shelf oxygen sensor, and involves only air and nitrogen gas. Using this technique, the in-plane effective diffusion coefficients in gas diffusion layers typically used in fuel cell electrodes were measured as a function of compression and hydrophobic polymer loading. As anticipated, with higher compressions and higher polytetrafluoroethylene (PTFE) loadings, effective diffusivity decreased, as a result of less pores space available for transport and because tortuosity increased. When plotted against compressed porosity, the effective diffusivity of untreated and treated materials for a given type of sample collapsed on top of each other, despite the simultaneous impact of PTFE-loading and compression. It was possible to distinguish between the impact of PTFE and compression by plotting the data as tortuosity against compressed thickness. High compressions on the sample lead to irreversible damages to the fiber structure, resulting in decreased or unexpectedly low tortuosity. Finally, a percolation model was fitted through results obtained from one of the tested materials and a reasonable agreement was observed for lower compression, but a fit to the entire data could not be achieved. This was attributed to fundamental structural changes occurring in the sample upon high compressions, an observation that helps to explain the general inability of theoretical tortuosity models to describe GDLs.

Résumé

La thèse présente une nouvelle technique expérimentale pour mesurer les composants en-plane des tenseurs de diffusivité dans les matériaux poreux minces. La méthode est basée sur la diffusion d'oxygène provenant de l'air dans un échantillon poreux qui a été purgé avec de l'azote. La concentration d'oxygène transitoire est mesurée à une position fixe dans l'échantillon. La réponse est analysée utilisant la loi de Fick pour la diffusion transitoire en une dimension. La teneur d'échantillon est conçue pour permettre des changements en compression, qui peut changer la porosité et sinuosité du matériel. La méthode conçue fournit des mesures précises, rapides et reproductibles, pouvant être appliquée à des matériaux conducteurs, utilise un teneur d'échantillon simple et un capteur à oxygène facile à obtenir, et implique seulement l'azote et l'air comme gases. La technique a été utilisée pour mesurer les coefficients de diffusivité en-plane des couches de diffusion de gas dans les piles à combustibles typiques. Les diffusivités sont mesurées en fonction de la compression et du chargement de polymère hydrophobique. La diffusivité monte avec de plus hautes compressions et plus de polytetrafluoroethane (PTFE) et diminue avec moins d'espace poreux et plus de tortuosité. Une relation entre la diffusivité effective et la porosité comprimée a été trouvée et ne semble pas affecter par la chargement de PTFE ou la compression. L'effet du chargement de PTFE et de la compression a été obtenue en utilisant les relations entre tortuosité et l'épaisseur comprimée. De fortes compressions endommagent la structure fibre de l'échantillon, ce qui diminue la tortuosité. Avec les résultats obtenus en faible compression, un modèle de percolation a pu représenter la réponse du matériel. Les résultats avec des compressions élevées n'ont pas pu être modélisés, ce qui est attribué à des changements structuraux. Ces résultats aident à expliquer la difficulté à représenter les couches de diffusion de gas avec des modèles de tortuosité.

Acknowledgements

First and foremost, I thank my supervisor Jeff Gostick for giving me the opportunity to join his research group and for his support, guidance and expertise. I am very thankful for putting his trust in me.

Secondly, I thank Jonathan Unno for his dedicated work in the lab, especially for building the porosity measurement setup and performing the measurements.

Thirdly, I would like to thank my research group mates Greg, Matt, Dave, and Mahmoud for the needed coffee breaks, lively discussions, sportsmanship, and comradeship throughout my time at McGill.

Lastly, for their continuous support, love, and encouragement, I thank my parents, my sister Sophia, and Alison Porter.

This research project would not have been possible without the generous funding provided by the Natural Sciences and Engineering Research Council (NSERC) and particularly by the Automobile Fuel Cell Corporation (AFCC). Their financial support is greatly appreciated.

Preface and Contribution of Authors

This thesis is submitted in compliance with the McGill University thesis preparation and submission guidelines and is formatted as a manuscript based thesis. In Chapter 1:, the thesis topic is introduced, followed by the thesis objectives. Chapter 2: includes the developed experimental method, validation, and comparison with experimental literature results. This work was submitted to the *Journal of International Heat and Mass Transfer* with Rinat Rashapov, Fariha Imani, and Jeff T. Gostick as authors [1]. Chapter 3: emphasizes on the results obtained with the newly developed technique and was submitted to *Transport in Porous Media*, authored by Rinat Rashapov and Jeff Gostick [2]. Chapter 4: completes the thesis and contains final conclusions and recommendations.

Porosity measurements were performed by Jonathan Unno, which were included in a separate study submitted and accepted to *Journal of The Electrochemical Society*, authored by Rinat Rashapov, Jonathan Unno, and Jeff T. Gostick [3]. All other experimental work and data analysis was performed by Rinat Rashapov who first-authored above mentioned manuscripts. Jeff Gostick provided expertise and guidance through editing and reviewing.

Prof. Jeff Gostick

Table of Contents

Abstract	ii
Résumé.....	iii
Acknowledgements.....	iv
Preface and Contribution of Authors.....	v
Table of Contents	vi
Table of Figures	viii
Table of Tables.....	x
Chapter 1: Thesis Introduction	1
1.1. Background	1
1.2. PEM Fuel Cells.....	2
1.2.1. Historic Background	2
1.2.2. Operating Principle	3
1.2.3. Performance.....	5
1.2.4. Water Management.....	7
1.2.5. Gas Diffusion Layer	8
1.3. Diffusion in Porous Materials.....	9
1.4. Thesis Objectives.....	11
Chapter 2: Method for Measuring In-Plane Effective Diffusivity in Thin Porous Media	13
Preface	13
2.1. Abstract	13
2.2. Introduction	14
2.3. Experimental	18
2.3.1. Setup	18
2.3.2. Procedure.....	19
2.3.3. Data Analysis.....	20
2.3.4. Thickness and Porosity.....	23
2.3.5. Validation	24

2.4.	Results and Discussion	26
2.5.	Conclusions	30
2.6.	Acknowledgements.....	31
Chapter 3:	In-plane effective diffusivity of gas diffusion layers for PEMFCs	32
	Preface	32
3.1.	Abstract	33
3.2.	Introduction	33
3.3.	Experimental	37
3.3.1.	Method	37
3.3.2.	Thickness and Porosity.....	39
3.3.3.	Materials	40
3.4.	Results and Discussion	41
3.4.1.	Effective Diffusivity.....	42
3.4.2.	Tortuosity	44
3.4.3.	Thickness Ratio	46
3.4.4.	Comparison with Percolation Theory	50
3.5.	Conclusions	55
3.6.	Acknowledgements.....	57
3.7.	Appendix	58
Chapter 4:	Final Conclusions & Recommendations.....	61
References	63

Table of Figures

Figure 1: Schematic of a fuel cell assembly including components and their respective dimensions.	4
Figure 2: Cell voltage (left) and power density (right) as a function of current density for open cell circuit and various polarizations.....	6
Figure 3: SEM images of untreated SGL 25AA (left, through-plane view) and untreated TGP-H-120 GDL (right, in-plane view).	8
Figure 4: Schematic of a PEMFC assembly illustrating mass transport and phase change mechanisms inside a fuel cell.....	15
Figure 5: Edge-view of the experimental setup for the determination of in-plane diffusivities of gas diffusion layers. Top: End view. Bottom: Side view. (Not to scale).....	18
Figure 6: Concentration profiles inside sample with time as a parameter.	21
Figure 7: Bulk diffusion coefficient D_b of oxygen in nitrogen at various shim thicknesses δ	25
Figure 8: Oxygen concentration vs. diffusion time curves of single-ended vs. double-ended open air diffusion.	26
Figure 9: Normalized effective diffusivity D' vs. porosity ε and tortuosity τ vs. porosity ε of untreated SGL 24AA and SGL 25AA.	27
Figure 10: Normalized effective diffusivity D' vs. porosity ε and tortuosity τ vs. porosity ε of untreated SGL 34AA and SGL 35AA.....	28
Figure 11: Normalized effective diffusivity D' vs. porosity ε and tortuosity τ vs. porosity ε of untreated SGL 24AA and PTFE treated SGL 24DA.....	29
Figure 12: SEM micrographs of untreated SGL 25AA, TGP-H-120, and Freudenberg H2315. Images on the right show a magnified view.....	35
Figure 13: Schematic of the experimental setup to measure the effective diffusivities of GDLs.....	38
Figure 14: Normalized effective diffusivity D' vs. compressed porosity ε of untreated and	

treated SGL 24, SGL 25, TGP-H-120 and Freudenberg H2315.....	43
Figure 15: Tortuosity τ vs. compressed porosity ε of untreated and treated SGL 24, SGL 25, TGP-H-120 and Freudenberg H2315.	45
Figure 16: Tortuosity τ vs. thickness ratio δ_0/δ of untreated and treated SGL 24, SGL 25, TGP-H-120 and Freudenberg H2315. Lines through data points are to guide the eye only.	47
Figure 17: Schematic illustration comparing the impact of compression and PTFE loading for two different samples at two different compression ratios, C_R	48
Figure 18: Measured tortuosity vs. thickness ratio of tested untreated (left) and 20 wt-% PTFE-treated (right) GDL materials.	50
Figure 19: Fitted percolation model through measured tortuosities vs. thickness ratio (left) and determined α -values vs. compressed porosity (right) of untreated and treated TGP-H-120.....	52
Figure 20: Predicted trends in tortuosity as a function of thickness ratio with PTFE loading as a parameter, indicated by the solid colored curves. The horizontal dashed lines are isolines of constant porosity, while the sloping dashed rules are isolines of constant normalized effective diffusivity. Experimental data points are included for comparison and color-coded according to PTFE loading.....	54
Figure 21: Normalized effective diffusivity D' vs. compressed porosity ε of untreated and treated SGL 34, SGL 35, TGP-H-060, and TGP-H-060.....	58
Figure 22: Tortuosity τ vs. compressed porosity ε of untreated and treated SGL 34, SGL 35, TGP-H-060, and TGP-H-060.	59
Figure 23: Tortuosity τ vs. thickness ratio δ_0/δ of untreated and treated SGL 25, SGL 35, TGP-H-060, and TGP-H-060.	60

Table of Tables

Table 1: GDL Samples used for In-plane Diffusivity Measurements.....	24
Table 2: Thickness, Porosity, and PTFE Loadings of tested GDL Materials.....	40

Chapter 1: Thesis Introduction

1.1. Background

Our society depends strongly on energy. The human population is growing rapidly, as is total primary energy demand per capita. By 2055, the world's population is estimated to increase by 30% to approximately 9.6 billion, putting more burden on global energy supply and energy infrastructure [4, 5]. Currently, the world's energy consumption is roughly fractioned into 88% fossil fuels, 5% nuclear energy, 6% hydro, and 1% into renewable energies [6]. In 2012, fossil fuels were divided into 33% oil, 30% coal, and 23% natural gas relative to total energy consumption [6]. These facts illustrate our high reliance on fossil energy sources, whose reserves are limited in supply and will ultimately deplete. This is generally projected to occur within our lifetime, though new fossil fuel explorations, enhanced-oil recovery techniques, and supply control may extend this time-frame for a limited period.

In 1956, King Hubbert published a significant article [7], in which he accurately predicted a bell-shaped oil production curve in the United States to occur in 1970, also known as "peak oil". Hubbert also applied his theory to the world's oil production and estimated a peak oil production around the year 2000 [8], though his prediction turned out to be incorrect, since geopolitical and economic factors as well as advances in technology were not considered. Nonetheless, it is now widely accepted, including by oil producing companies and organizations such as OPEC, that world oil production will pass a peak, although the timeframe is still under dispute [9]. This concerning fact, in addition to the significant contributions of fossil fuels to the emission of greenhouse gases (GHGs), has motivated the search for alternative fuels and energy sources. The United Nations Framework Convention on Climate Change (UNFCCC), as the most significant international treaty on climate change, has set the objective to stabilize "greenhouse gas concentrations in the atmosphere at a level that would prevent dangerous anthropogenic interference with the climate system" [10]. In order to cope with the inevitable depletion

of fossil fuels and growing energy demand, while simultaneously meeting GHG emission targets, much focus has been laid into the development of alternative and renewable energies such as wind, solar and hydro-power, geothermal energy, and biomass energy.

The fuel cell plays a key role in the “hydrogen economy” vision, in which hydrogen produced from non-fossil fuels is expected to substitute conventional fossil fuels used in internal combustion engines (ICEs). Proton exchange membrane fuel cells (PEMFCs) represent a promising alternative energy technology, specifically for portable, mobile, and automotive applications, since they exhibit high power densities and quick refueling times, and thus, are able to compete with conventional ICEs. Recent research in fuel cell technology, specifically due to the development of new catalysts with lower platinum loadings and more effective membrane materials, has significantly improved the efficiency, viability, and cost-effectiveness of PEMFCs. Many major automotive manufacturers have recognized the high potential of PEMFCs and developed prototype cars based on fuel cell technology [11]. The automotive industry expects fuel cell vehicles to be commercially available within the next 3-5 years, though further improvements are still necessary. These challenges include implementing a hydrogen supply infrastructure, and further increasing PEMFC performance. Improving the performance of fuel cells directly leads to cost reduction, as less catalyst and membrane materials are required to generate the same amount of power, therefore, also reducing fuel cell stack size and total weight. Performance can also be increased by reducing voltage losses and thus, increasing fuel use efficiency. These improvements are particularly of interest for the automotive industry, which uses pressurized tanks to store a limited amount of hydrogen.

1.2. PEM Fuel Cells

1.2.1. Historic Background

In 1839, William Grove performed an experiment in which he placed two platinum electrodes in an aqueous sulfuric acid solution and observed the evolution of hydrogen gas on one electrode and oxygen gas on the other [12]. This finding started the fuel cell

technology and inspired German chemist Christian Schönbein [13], who performed the first scientific research on the fuel cell and published his findings in a scientific journal [14]. In 1889, a fuel cell prototype was built by Ludwig Mond and Carl Langer [12], while the first commercial fuel cell was developed in 1955 by GE, NASA, and McDonnell for the application in NASA's Gemini space program [14]. However, due to the fuel cell's inefficiency, low reliability, and high cost at that time, fuel cells remained a niche technology and were abandoned in the 1970s. From the mid-1980s, however, fuel cells went through a renaissance due to significant cost-reductions and awareness of depleting fossil fuels. Since then, fuel cells became increasingly popular and have been implemented in various mobile (aircrafts, cars, busses, trucks, boats, and forklifts) and stationary applications (vending machines, source of emergency power, and electricity source in remote and isolated locations).

1.2.2. Operating Principle

PEMFCs are galvanic cells, which generate pure water, waste heat and electricity as a result of an electrochemical conversion of hydrogen and oxygen gas. Figure 1 illustrates a schematic of a single PEM fuel cell including internal components and their dimensions. A PEMFC is comprised of two components: Two bipolar plates and the membrane electrode assembly (MEA). The MEA includes the gas diffusion layer (GDL) and catalytic layer (CL) for both cathode and anode, and the electrolyte membrane (EM), separating both electrodes. In order to conduct generated electricity, the bipolar plates are made from graphite or metal material, into which serpentine flow channels are stamped or engraved. The GDL is a thin, fibrous, and porous carbon paper and allows for reactant gases to distribute uniformly into catalyst regions located under the channel ribs. Moreover, it serves as a current collector and gives access to electrons to the catalyst layer located under the channels. A more detailed description of the GDL is shown below. The catalyst layer contains a mixture of carbon-supported platinum particles and ionomer. Similar to the GDL, the catalytic layer is also porous to allow for gas transport to and from the active sites, while carbon particles and ionomer provide pathways for generated

electrons and protons, respectively. Coolant channels in the bipolar plates remove the generated waste heat. The operational temperature of PEMFCs range from 50 to 100 °C.

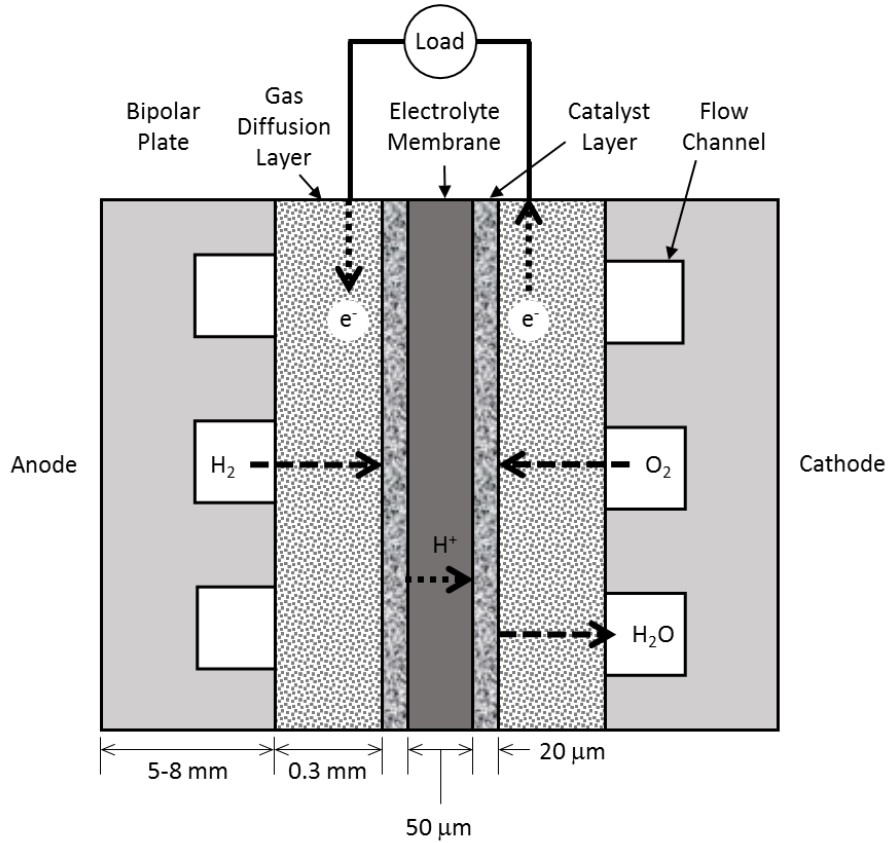


Figure 1: Schematic of a fuel cell assembly including components and their respective dimensions.

During operation, humidified hydrogen gas is supplied from a pressurized hydrogen tank to the serpentine flow channels engraved in the anode bipolar plate and diffuses through the GDL towards the anode CL. At anode catalyst sites, molecular hydrogen is oxidized to protons:



Due to the unique nature of the Nafion membrane, protons are capable of dissolving within the electrolyte and are subsequently conducted through the membrane towards

the cathode. Additionally, the electrolyte material has a lower permeability to gas and prevents reactants from mixing with each other. The generated electrons are diverted onto an external circuit, thus, creating a direct electric current.

On the cathode side, oxygen gas or air reaches the catalyst layer through similar transport processes and molecular oxygen is reduced to oxide:



Protons conducted through the electrolyte membrane subsequently recombine with oxide ions, thus, yielding pure water. The overall reaction is therefore:



Gaseous or condensed product water at the cathode then diffuses through the GDL back to the flow channels in the cathode BP and is finally removed by the oxygen (or air) gas stream.

1.2.3. Performance

The overall reaction stated in Eq. (3) generates a theoretical Nernst potential of 1.223 V, which is the theoretical maximum cell voltage, assuming no energy losses occur during operation. In order to obtain higher voltages, individual fuel cells are stacked in series until the desired output voltage is reached. The output power, P , of a fuel cell can be determined through multiplying the voltage, V , with the electric current, I . The open circuit voltage represents the maximum cell voltage when no current is drawn and therefore is equal to 1.223 V. However, during fuel cell operation, several voltage losses occur, effectively limiting the cell voltage and fuel cell performance. These losses can be split up into three components: activation polarization, resistance (Ohmic) polarization, and concentration polarization. Figure 2(left) illustrates four different polarization curves

of a PEMFC, while Figure 2(right) shows the corresponding power density for each case as a function of current density. The solid line represents the open circuit voltage, which remains constant for all current densities, as no current is drawn. Activation polarization losses occur at the catalytic electrode, specifically at the cathode, due to limiting kinetic effects such as charge transfer, adsorption, desorption, and formation of intermediates. Ohmic losses arise as a result of electric resistance caused by limitation of electron mobility occurring during proton transport in the electrolyte membrane and electron conduction through the current collector and other conductive materials. Ohmic losses are particularly problematic at high current densities. As shown in Figure 2, concentration polarization has a significant impact on the fuel cell performance, since cell voltage losses due to mass transport limitations cause a substantial drop in cell voltage and ultimately place an upper limit to the achievable current density in a fuel cell.

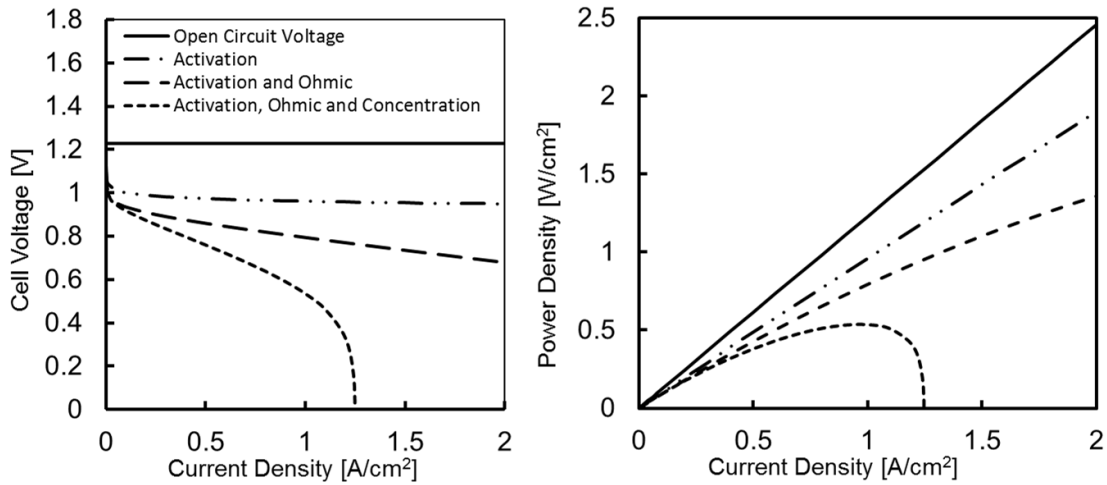


Figure 2: Cell voltage (left) and power density (right) as a function of current density for open cell circuit and various polarizations.

At such high current densities, reactants at the catalytic layer are consumed at a faster rate than can be supplied through the GDL and the maximum power density and therefore overall performance of a fuel cell is significantly limited. It is clear that by reducing mass transport resistance, maximum current density increases and the fuel cell performance is improved. As a result, mass transport constraints represent a major issue during fuel cell

operation and it is of great importance to fully understand and study such limitations with the aim of improving cell efficiency.

1.2.4. Water Management

Generation of only pure water as the sole reaction product represents a strong advantage of PEMFCs compared to internal combustion engines, emitting water and environmentally harmful carbon oxides and nitrogen oxides. Simultaneously though, water production in fuel cells represents a major engineering challenge, as the product water needs to be continuously removed from the cell, while supplying the cathode catalyst layer with sufficient oxygen to maintain the electrochemical reaction. A “drying out” of the cell must be avoided though, as a certain degree of humidity in the cell facilitates the proton transport in the electrolyte membrane. Conversely, excessive humidity causes a “flooding” of the cell and the reaction would halt due to an extreme increase in mass transfer resistance. Thus, controlling the humidity of the fuel cell is of significant importance to fuel cell performance and is referred to as water management.

A common technique to remove extensive water from the cell is to coat the GDL with a hydrophobic polymer, such as PTFE. The polymer is deposited onto the fibers and effectively repels water, which is finally removed from the GDL through the continuous oxygen (or air) stream in the bipolar plate. However, extensive PTFE loadings reduce the porosity of the GDL significantly and are contra-productive, as mass transport rates decrease with lower porosities. A second method to improve water management in fuel cells is to treat the macro-porous GDLs with a micro-porous layer (MPL), which is made from carbon agglomerates and is applied to the interface between the GDL and the catalytic layer. The MPL consists of a powder mixture of carbon and PTFE, which is added to the GDL surface and sintered to bind GDL and MPL together. Even though the MPL exhibits much smaller pore sizes than the GDL, it demonstrated an improvement in water removal, electric conductivity, and mechanical stability [15]. However, the exact mechanism for these enhancements are still not fully understood [16].

It is clear that the control of humidity inside the cell is of significant importance to the occurring transport processes such as mass, electron, and proton transport. Therefore, water management directly dictates fuel cell performance and efficiency.

1.2.5. Gas Diffusion Layer

Gas diffusion layers are manufactured as porous sheets of 150-400 μm thickness and consist of fibrous graphite carbon paper or cloth. As illustrated in the assembly schematic shown in Figure 1, an individual cell contains two GDLs, one for each electrode. Their main purposes include the provision of mechanical stability to the catalyst layer, controlling of water management within the cell, conduction of generated electricity and waste heat, and uniform distribution of reactants onto the catalyst layer. SEM micrographs of a typical GDL are illustrated in Figure 3. Additional SEM images of various GDLs are included in Chapter 3:.

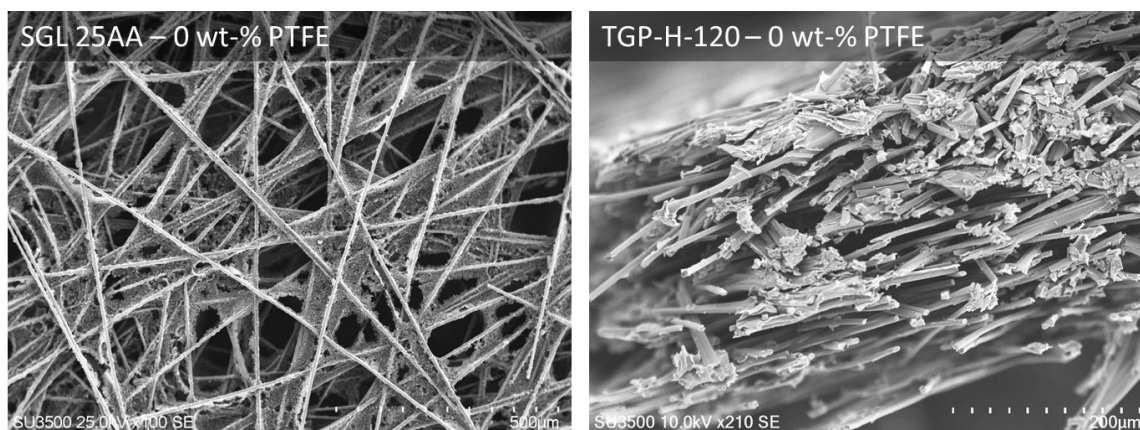


Figure 3: SEM images of untreated SGL 25AA (left, through-plane view) and untreated TGP-H-120 GDL (right, in-plane view).

The GDL provides mechanical stability to the catalyst layer, as it separates the bipolar plates from the catalyst layer and therefore prevents direct contact, as this would wear off the catalyst and significantly reduce its performance. The presence of the GDL is especially important, since small compressions are generally applied to the GDL in order

to obtain good connectivity between each components. As mentioned in the previous section, the GDL is generally sintered with hydrophobic PTFE in order to improve water management. It has been found that a PTFE-loading of approximately 10-20 wt-% is optimal and keeps water removal, humidity, and effective diffusion transport in balance. While diffusive mass transport occurs through the open pores, electrons are conducted to and from the reaction site through the solid matrix of the GDL. The porosities of GDLs range approximately between 70-90%. Furthermore, GDL thickness plays an important role during the electron conduction and mass transport, as thinner materials reduce the conduction pathway and therefore decrease Ohmic losses, while simultaneously improving reactants and water transfer.

Perhaps most importantly though, the GDL improves effective transport and conductivity of reactants and electrons between the channels and ribs of the bipolar plates and the catalyst layer. Uniform reactant distribution onto the catalyst layer is crucial for cell performance and is ensured through the presence of the GDL. While the catalyst regions directly located under a flow channel are fully exposed via through-plane (TP) diffusion of oxygen and hydrogen gas, catalytic reactive centers located under the channel ribs run the risk of being undersupplied of reactants. Therefore, effective in-plane (IP) diffusion inside the GDL matrix is necessary to fully expose these areas.

1.3. Diffusion in Porous Materials

Diffusion of solid, liquid, or gaseous species occur as a results of an existing concentration gradient. The diffusion coefficient or diffusivity, D , is a proportionality constant between the molar flux and the concentration gradient and describes at what rate two species mix with each other. The diffusion coefficient can be determined from Fick's law:

$$J = -D \frac{\partial C}{\partial z} \quad \text{Eq. (4)}$$

where J represents the diffusion flux, C the concentration of the diffusive species, z the

spatial domain, and D the diffusion coefficient. Fick's Second Law for transient, one-dimensional diffusion is:

$$\frac{\partial C}{\partial t} = D \frac{\partial^2 C}{\partial z^2} \quad \text{Eq. (5)}$$

where C is the concentration in mol/unit volume, z is the spatial coordinate along which the concentration gradient exists, t is the time, and D is the diffusion coefficient. The diffusion coefficient depends heavily on temperature and pressure and is generally reported as bulk or binary diffusion coefficient, D_b , or D_{AB} , respectively. Fuller et al. [17] developed an expression to estimate the binary diffusion coefficient, D_{AB} , of two gaseous species as a function of temperature, T , and pressure, p :

$$D_{AB} = \frac{10^{-8} T^{1.75} \left(\frac{1}{M_A} + \frac{1}{M_B} \right)^{1/2}}{p [(\sum_A v_i)^{1/3} + (\sum_B v_i)^{1/3}]^2} \quad \text{Eq. (6)}$$

where M_A and M_B represent the molecular mass of species A and B, respectively and v_i represents tabularized diffusion volumes.

Porous materials, such as sandstone, rocks, soil, zeolites, cements, and ceramics reduce the binary diffusion coefficient, as diffusing particles are hindered by the solid matrix. This reduction in diffusivity is accounted for in the effective diffusivity, D_{eff} . In porous materials, Fickian diffusion is a valid concept for describing effective diffusion in macro-pores exhibiting a pore diameter >50 nm, however, for micro-pores (< 2 nm), interactions between the pore wall and the diffusing particles are more dominant. In this regime, Fickian diffusion transitions over to Knudsen diffusion and the diffusion coefficient can be determined through kinetic gas theory. Knudsen diffusion is not a factor in the large pore of the GDL, but may be important if an MPL is present. The porosity, ε , of porous media is a crucial dimensionless parameter and gives a measure of open pore space available for mass transport in the material. The uncompressed porosity, ε_0 , of a porous sample can be

calculated as:

$$\varepsilon_0 = 1 - \phi_s = \frac{V_s}{V_b} \quad \text{Eq. (7)}$$

where ϕ_s is the solid fraction and V_s and V_b are the solid and bulk volume of the porous sample, respectively. Effective diffusivity is given by:

$$D_{eff} = D_{AB} \frac{\varepsilon}{\tau} \quad \text{Eq. (8)}$$

where ε is the porosity of the media ($\varepsilon < 1$) and τ is the tortuosity ($\tau > 1$), accounting for the increased path lengths of diffusion molecules around solid obstacles relative to the length of the domain [18-21]. Effective diffusivity can be normalized by forming the ratio with D_b , resulting in the normalized effective diffusivity, D' .

1.4. Thesis Objectives

Various studies on GDLs have been reported in the literature, concentrating on a wide spectrum of parameters which determine the rate of gas diffusion through such porous materials. These features include thickness, porosity, degree of PTFE loading, pore orientation, effect of mechanical compression, electrical and thermal conductivity, pore-size distribution as well as tortuosity. While a high number of studies apply a purely theoretical approach to determine mass transport characteristics in GDLs, experimental results are scarce, and as a result, theoretical models cannot be tested in their validity. Therefore, it is crucial to obtain experimental data to improve the understanding of effective mass transport in porous fuel cell electrodes.

The objective of this thesis was to experimentally study effective mass transport through thin, porous media such as GDLs and to contribute to the understanding of transport limitations occurring in PEMFCs. Ultimately, these findings are expected to help reduce

mass transport resistance and improve the current maximum power density of PEMFCs, therefore, also increasing fuel cell performance and efficiency. The goals of this thesis can be summarized as follows:

- Develop and validate experimental diffusion technique to measure in-plane effective diffusion coefficients of thin, porous materials in a straight-forward, accurate, and fast manner.
- Determine effect of compression on effective diffusivity and tortuosity of oxygen gas in gas diffusion layers.
- Determine impact of GDL additives such as PTFE and binder on effective gas transport characteristics.
- Compare results with experimental data and models reported literature.

Chapter 2: Method for Measuring In-Plane Effective Diffusivity in Thin Porous Media

Preface

In Chapter 2;, a new experimental technique in order to measure the in-plane effective diffusion coefficient of thin, porous materials such as gas diffusion layers used as fuel cell electrodes is established and compared with literature. This study was submitted and accepted to the *International Journal of Heat and Mass Transfer* and primarily focusses on the development and validation of the experimental technique. The work is authored by Rinat Rashapov, Fariha Imani, and Jeff T. Gostick [1]. In addition, detailed data analysis required to obtain the effective diffusivity is presented.

2.1. Abstract

A new experimental technique for measuring the in-plane components of the effective diffusivity tensor of thin porous materials is presented. The method is based on the transient diffusion of oxygen from air into a porous sample initially purged with nitrogen. The oxygen concentration is measured at a fixed location in the sample with time and the response is fitted to an analytical solution of Fick's law for one-dimensional, transient diffusion. As validation, it was confirmed that this method reproduced the theoretical value of oxygen diffusivity in nitrogen within 1% when no sample is present. Effective diffusion coefficients were measured for a variety of thin fibrous graphite paper materials typically used in fuel cell electrodes. The sample holder was designed to allow varying degrees of compression, thereby changing the porosity and tortuosity of the material. As expected the effective diffusivity drops with compression, not only due to a decrease in porosity but also to a large increase in tortuosity. The present method provides accurate, fast, and repeatable measurements, is applicable to electrically conductive materials where brine conductivity is difficult to interpret, uses a simple sample holder, an off-the-shelf oxygen sensor, and involves only air and nitrogen gas. The obtained values were in excellent agreement with comparable results in the literature, yet with a much more

direct method.

2.2. Introduction

Global fossil energy resources are expected to be largely depleted within our lifetime [7]. This troubling fact, in addition to their contribution to the emission of greenhouse gases, has motivated the search for alternative fuels and energy sources. The hydrogen fuel cell is a major component of this vision, since hydrogen can be easily produced from many different methods, such as reforming natural gas or biogas [22, 23], electrolyzing water using wind power or solar farms [24], or even splitting molecular water using solar powered photolytic reactions [25]. Hydrogen fuel cells, also known as Polymer Electrolyte Membrane Fuel Cells (PEMFCs), are particularly promising for mobile and automotive applications due to their high power density and quick refueling times, comparable to internal combustion engines. Most major automotive manufacturers have committed to offer fuel cell vehicles commercially between 2015 and 2020 [26].

Figure 4 illustrates a schematic cross-section of a fuel cell assembly showing the flow field plates, the gas diffusion layer (GDL), catalyst layer (CL), and the polymer electrolyte membrane (PEM). Also shown schematically in Figure 4 are the many transport mechanisms that occur simultaneously through the various porous components during cell operation. A detailed description of PEM fuel cell operation can be found elsewhere in review articles [27, 28] and textbooks [29, 30]. One of the more important transport processes is the diffusion of gaseous reactants from the flow channels through the GDL to the CL. The GDL plays many roles inside the PEMFC, including conduction of heat and electrons and provision of mechanical support to the soft membrane. However, as the name suggests, their primary purpose is to disperse gaseous reactants from the flow channels to regions of the catalyst layer under the ribs. The rate at which gas diffuses through the GDL is directly linked to the amount of electric current generated, but also impacts the efficiency of cell operation through the phenomena of concentration polarization [24]. It is consequently of great importance to properly characterize the gas

diffusivity of these materials, with the aim of reducing mass transport limitations and increasing fuel cell efficiency. Engineering the fuel cell to operate at higher current density means that cells can be made smaller and more cost-effective for a given power rating, and operating at high efficiency means longer ranges between refilling.

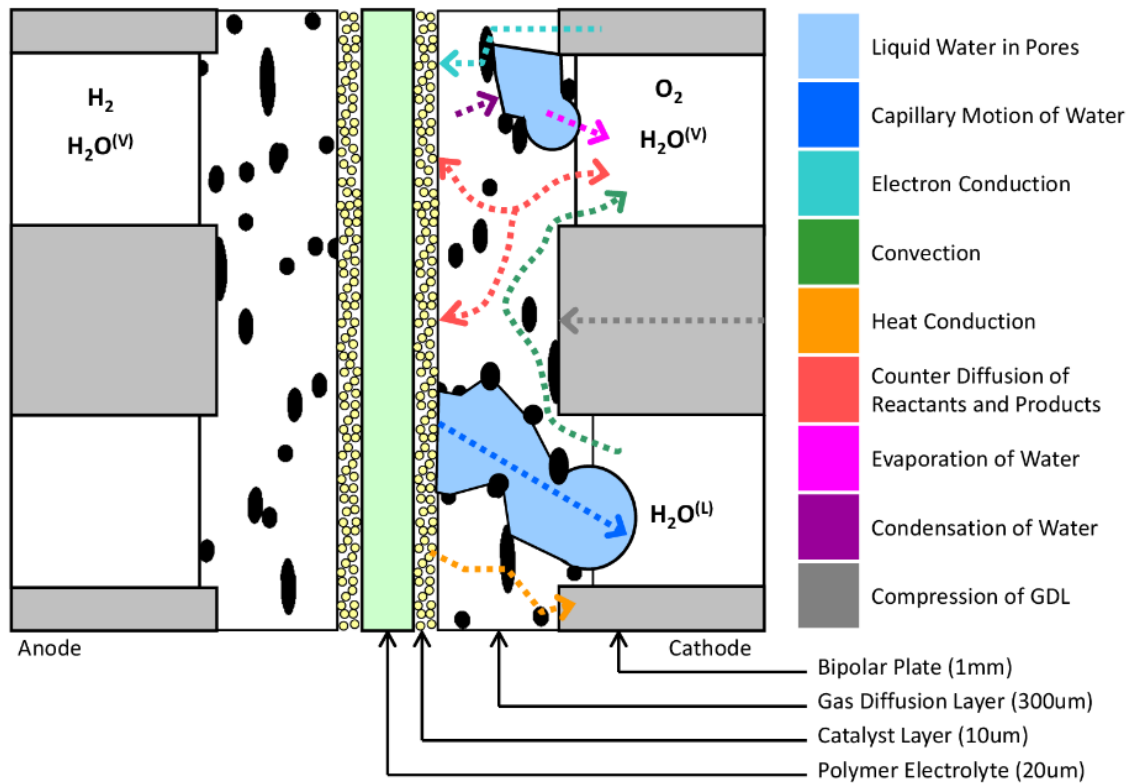


Figure 4: Schematic of a PEMFC assembly illustrating mass transport and phase change mechanisms inside a fuel cell.

There are two main difficulties with measuring the effective diffusivity in the GDL. Firstly, the materials are very thin, making it challenging to apply controlled boundary conditions. For instance, their high permeability combined with their minimal thickness mean that even slight pressure differences cause significant convective flows. Secanell and co-workers [31] have developed a Wicke-Kallenbach type cell for measuring through-plane (TP) diffusivity, but this was only feasible for materials with a microporous layer (MPL), whose low permeability buffered against pressure fluctuations. Even so, this type of setup

requires very careful control of the pressure, composition, and flow rates on each face of the sample. The second difficulty is that GDLs are electronically conductive. Therefore, the standard porous media approaches based on measuring brine conductivity to infer formation factor [32, 33] will not work directly, as the ionic and electronic transport must be accounted for. Büchi and co-workers [34] have developed a sophisticated technique using electrochemical impedance spectroscopy to de-convolute the effects of these two transport mechanisms. Not only is this method somewhat complex and difficult to reproduce for non-electrochemists, it does also not actually measure effective diffusivity directly.

A variety of other experimental approaches have been taken in attempts to study the GDL. Astrath et al. [35] developed a Loschmidt method [36] to study diffusion through porous separators and membranes, and this group subsequently studied the TP effective diffusivity of GDL materials [37]. This approach involves allowing two separate gas chambers with differing initial concentrations to counter-diffuse into each other. When the chambers are separated by the GDL, gases must diffuse through it, thereby adding a diffusive resistance to the process. Quick et al. [38] and LaManna et al. [39] developed an experimental technique to measure the effective diffusivity of water vapour, by creating a humidity gradient in the porous sample via a dry and a humidified flow channel. A similar approach was used by Baker and co-workers [40] but without flow. Utaka et al. [41] built an electrochemical oxygen sensor to measure the effective diffusion coefficient of microporous media under dry and wet conditions. This technique was interesting, since the electrochemical oxygen sensor consumed oxygen to establish a stable concentration gradient through the sample. Moreover, the current produced by the sensor indicated the flux, and the voltage of the sensor provided the concentration. This approach required manufacturing a custom made oxygen sensor, and the kinetics were still relatively slow, thus requiring several millimeter of sample to create a noticeable gradient. Baker et al. [40] have also attempted to measure diffusion rates inside running fuel cells by investigating the limiting current behavior. The difficulty with this approach is that the

production of liquid water inside the cell cannot be controlled or avoided, the resulting value includes some IP diffusivity effects, the contribution of the catalyst layer cannot be distinguished, and the impact of convection in the flow channel and the so-called Brinkman effect disturb the boundary conditions. In their study, Baker et al. used an in-situ limiting current method to measure the effective diffusion coefficient of oxygen gas through a GDL. A similar approach was used by Hwang and Weber [42], but instead they used a hydrogen pump reaction, where hydrogen gas is electrolytically converted into protons, and back into hydrogen at the reference electrode. These studies have looked at factors including sample thickness, porosity, degree of polytetrafluoroethylene (PTFE) loading, mechanical compression, temperature, and even liquid water content [37, 39, 42-44].

All of the above mentioned studies have focused on the TP direction, as diffusion in this direction ultimately controls the rate of reactant supply to the electrode. Fibrous materials like GDLs possess significant structural anisotropy due to the fiber orientation, so to fully characterize these materials, it is necessary to measure their effective diffusivity tensor. Diffusion in the IP direction is a critical factor for several reasons. This information is needed for 3D modeling studies of gas distribution and catalyst utilization within the cell, and also impacts engineering decisions such as the optimal channel-to-rib ratio and GDL thicknesses. Surprisingly few studies have been performed on GDLs in the IP direction. To date, the only IP diffusivity measurements have been performed using the electrochemical diffusimetry technique of Kramer et al. [34]. Although their results appear to be quite solid, it is of strong interest to develop an alternative and more widely accessible technique. In this present study, a new experimental method was developed and validated in order to measure the IP effective diffusion coefficient of various GDLs, including the influence of mechanical compression.

2.3. Experimental

2.3.1. Setup

The experimental setup consists of a sample holder, an oxygen sensor, and a N₂ flushing apparatus. The sample holder was constructed from two 1" thick stainless steel plates between which the porous sample was clamped as illustrated in Figure 5.

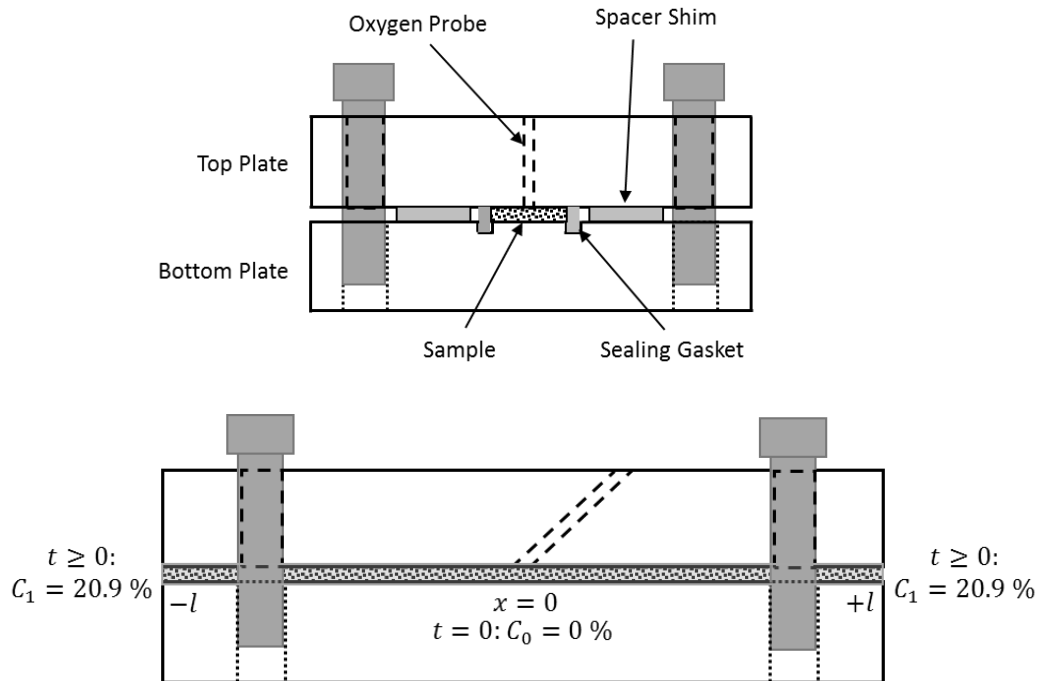


Figure 5: Edge-view of the experimental setup for the determination of in-plane diffusivities of gas diffusion layers. Top: End view. Bottom: Side view. (Not to scale)

The plates were polished with up to a 2000 grit sandpaper to a mirror finish to ensure that gas did not preferentially diffuse along the milling grooves present in the unpolished holder. The sample thicknesses were in the range of 178 μm to 264 μm , so a roughness of even a few dozen μm would represent a significant gap. Of course, the sample surfaces are themselves rough, but preferential diffusion along this path is an integral part of the material behavior. The samples were cut from larger sheets into 7.62 cm x 0.85 cm strips and then positioned at the center of the bottom sample holder plate. A pliable sealing material was placed on each long edge of the sample to prevent gas entrance into the

sides. When assembled, gas could only diffuse into the ends of the sample. Two spacer shims of equal thickness were placed between the plates on each side of the sample. The shims were accurate to within $\pm 1 \mu\text{m}$, and they ensured that the sample was compressed to a known thickness. An optical oxygen sensor (OceanOptics FOXY-NeoFox[®]) was installed at a fixed position in the top plate, extending down to the surface of the porous sample [45]. The sensor records the partial pressure of oxygen inside the porous sample. The oxygen probe was received pre-calibrated over a range of 0% to 21% oxygen, measured at eight different temperatures between 0°C and 30°C. Both ambient temperature and pressure are recorded and used to compensate for any temperature or pressure fluctuations during the measurements. These corrections were all performed by the NeoFox software, which outputs a final oxygen partial pressure value. All measurements were made at ambient laboratory conditions of approximately 22°C, 101 kPa and 35% RH.

2.3.2. Procedure

Prior to each diffusion measurement, the oxygen probe was tested to ensure a reading of 20.9% oxygen at the measured ambient temperature. The GDL sample was then gently flushed with nitrogen gas for approximately 1 minute to generate the zero-oxygen initial condition throughout the porous medium. The experiment began the moment the flushing stopped, since oxygen immediately began to diffuse through both ends into the sample. The transient oxygen concentration $C(t)$, was recorded for approximately 10 to 20 minutes, depending on the time required to reach atmospheric oxygen concentration inside the sample. After a constant value of 20.9% oxygen was recorded over several minutes, data acquisition was stopped. Figure 8 shows a typical experimentally measured oxygen concentration profile vs. time. For subsequent measurements, compression on the sample was increased by replacing the spacer shims by thinner ones, without disturbing the sample. By decreasing the sample thickness stepwise down to 76 μm , compressions up to of 70% could be achieved. The 1" thick sample holder plates did not bend or bow at these high compressions, and this was confirmed by taking micrometer

measurements of the sample holder outer dimensions. For each compression, the experiment was performed twice in order to ensure the reliability of each measurement.

2.3.3. Data Analysis

The experiment outlined above results in an oxygen concentration vs. time profile at constant position z . To extract the effective diffusivity of a porous material from this data, it is necessary to model this profile using Fick's Second Law for transient, one-dimensional diffusion:

$$\frac{\partial C}{\partial t} = D \frac{\partial^2 C}{\partial z^2} \quad \text{Eq. (9)}$$

Where C is the concentration in mol/unit volume, z is the spatial coordinate along which the concentration gradient exists, t is the time, and D is the diffusion coefficient. Eq. (9) can be analytically solved for the present diffusion problem by applying the following boundary conditions which are also illustrated in Figure 5(bottom):

$$C = C_1, z = \pm l, t \geq 0$$

$$\frac{\partial C}{\partial z} = 0, z = 0, t > 0$$

$$C = C_0, -l < z < l, t = 0$$

The solution for a plane sheet of length l with a uniform initial concentration C_0 , constant surface concentration C_1 , and a no-flux boundary condition at $z = 0$ is given by [46]:

$$\frac{C(t) - C_0}{C_1 - C_0} = \sum_{n=0}^{\infty} (-1)^n \operatorname{erfc} \frac{(2n+1)l - z}{2\sqrt{Dt}} + \sum_{n=0}^{\infty} (-1)^n \operatorname{erfc} \frac{(2n+1)l + z}{2\sqrt{Dt}} \quad \text{Eq. (10)}$$

Where l represents the domain length, z the position, and D the diffusion coefficient. The experimental setup described above corresponds to Eq. (10) when the sample is initially

flushed with pure N_2 , ($C_0 = 0$) and O_2 from air ($C_1 = 20.9\%$) is allowed to enter at time $t = 0$. $C(t)$ is the measured O_2 concentration in the sample at location z , which is measured by the oxygen probe. The only unknown in Eq. (10) is the diffusion coefficient D , which is found by least-squares fitting of Eq. (10) to the measured oxygen concentration. With a porous sample inside the sample holder, D_{eff} instead of D_b is obtained. The solution to the diffusion equation given by Eq. (10) is valid for small times but is also applicable for longer diffusion times, though more summation terms are required to achieve a stable solution than the corresponding 'long time' solution [46]. Figure 6(left) shows the oxygen profiles within the sample with each line representing a time step of 5 seconds. Figure 6(right) shows the predicted time dependent oxygen concentration at the sensor position. These theoretical results are plotted together with experimentally measured concentrations in Figure 8. The correspondence between the experiment and Eq. (10) is excellent.

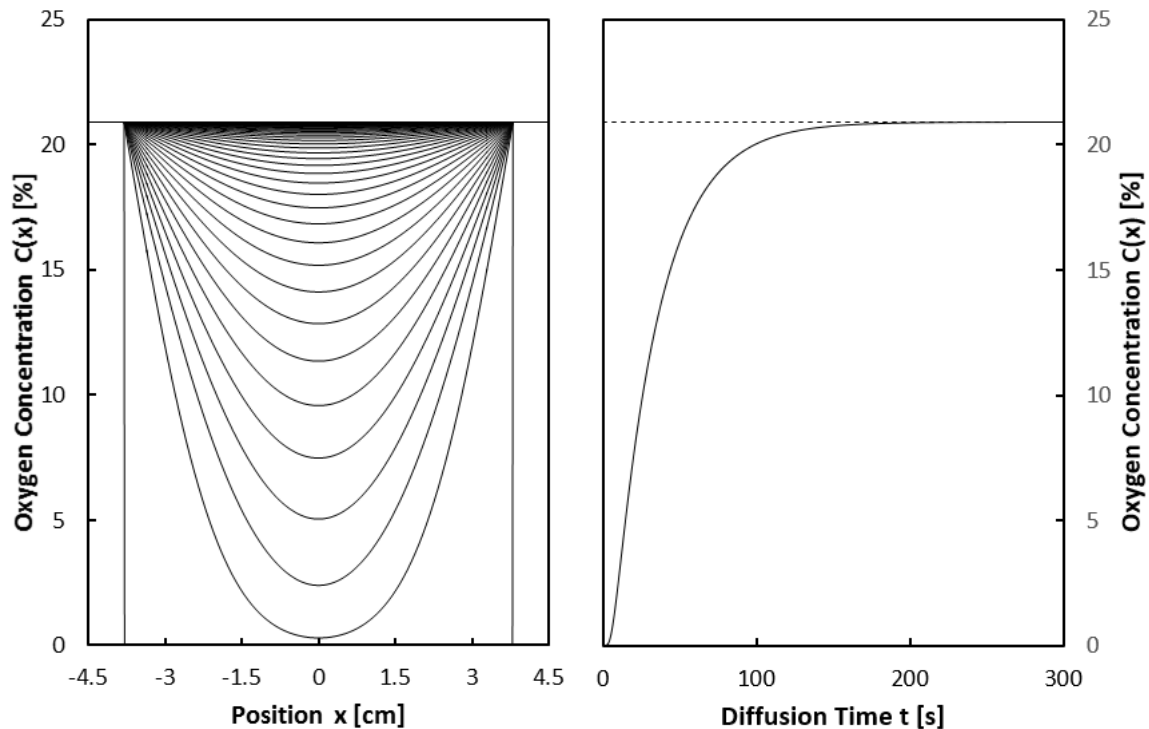


Figure 6: Concentration profiles inside sample with time as a parameter.

It is important to recognize that the effective diffusivity D_{eff} determined by fitting Eq. (10) is equal to D_b/τ and not $D_b\varepsilon/\tau$ as is almost universally used. The traditional definition of D_{eff} arises from the application of Fick's First Law for *steady-state* diffusion through a porous domain:

$$n = \frac{\varepsilon AD_b}{\tau} \frac{dC}{dz} = AD_{eff} \frac{dC}{dz} \quad \text{Eq. (11)}$$

Where n is the molar flow rate of the diffusing species, A is the superficial area of the domain normal to the direction of diffusion, and ε and τ are the porosity and tortuosity of the porous material, respectively. This is a convenient working definition of D_{eff} for steady-state cases, since the porosity has the effect of reducing the observed diffusion coefficient by reducing flux through the domain. It is also misleading, however, since it obscures the fact that the porosity term is accounting for geometric aspects of the calculation (such as reduced pore volume and total area for flow), and not the physical behavior of the diffusing molecules (which is accounted for by tortuosity). This confusion is highlighted in transient calculations, where the accumulation term must also be adjusted for porosity, since the pore volume is lower than the total domain volume by a factor of ε . The concentration C is the number of moles per unit volume of *domain*, so the actual number of moles in the domain is lower by a factor of ε . Consequently, for transient diffusion into a porous domain, both the flux into the domain and the total moles that accumulate are reduced by a factor of ε . This effectively means that both sides of Eq. (9) are to be multiplied by ε , which of course cancel out. The final result of these considerations is that the effective diffusivity in Eq. (10) is simply D_b/τ . This issue is discussed in detail by Shen and Chen [21].

The determination of tortuosity from Eq. (10) can also be accomplished by adjusting the domain size l to find an effective domain length l_{eff} , while setting D to the value of bulk air D_b . The effective domain length thus determined is related to tortuosity as [47, 48]:

$$\tau = \left(\frac{l_{eff}}{l} \right)^2 \quad \text{Eq. (12)}$$

Where l_{eff} is the effective length of the domain due to the increased diffusion path lengths, and l is the actual domain length in the absence of a porous material. Tortuosity is also often defined as $\tau = l_{eff}/l$, but as discussed in various sources [18-20], the appropriate definition depends on the form of diffusion equation being used. As can be seen in Eq. (10), the concentration is a function of the square-root of D , but a linear function of l . Hence, Eq. (12) is appropriate in this case. Using this approach, it is apparent that porosity is not a factor in the equation.

Delgado [49] developed a similar technique to measure the tortuosity in packed beds, based on the transient uptake of ions into a bed initially filled with pure water. In that work, the concentration boundary condition varied with time as ions moved into the bed, whereas in the present work, it is assumed that the oxygen at the boundary is replenished and is therefore constant throughout the experiment. The present approach has the advantage of working with the gas phase, thereby avoiding the need to completely saturate the sample, and it is very quick, taking just minutes compared to a day. It is also designed specifically for thin porous sheets under compression.

2.3.4. Thickness and Porosity

All tested GDL samples in this study were SIGRACET® GDL materials provided by SGL Group. These were chosen since comparable data was reported by Flückiger et al. [44]. Table 1 lists the properties of the tested GDL samples, including their measured thicknesses and porosities. The uncompressed thickness was measured at ten different locations using a micrometer with a resolution of 1 μm . The porosity was provided by the manufacturer, and these values were confirmed by Flückiger et al. [44] using independent measurements. These materials are named by SGL according to their Series, Generation, PTFE Loading, and MPL type. For instance, 24AA is series 2, generation 4, 0% PTFE, no MPL, while 34AA is series 3 which is thicker, but otherwise has the same configuration. In this work, series

2 and 3 materials were tested, generations 4 and 5 were compared, all samples had no PTFE (A) with one exception that had 20% (D). Only materials with no MPLs were considered (A).

Table 1: GDL Samples used for In-plane Diffusivity Measurements

Material	PTFE	δ_0	ε_0
	[wt-%]	[μm]	[-]
SGL 24AA	0	181	0.88
SGL 25AA	0	178	0.92
SGL 24DA	20	184	0.82
SGL 34AA	0	252	0.88
SGL 35AA	0	264	0.92

To illustrate the effect of mechanical compression on the diffusion coefficient of GDLs, it is helpful to plot the effective diffusivity values as a function of compressed porosity. The sample's porosity at any compressed thickness can be related to its initial thickness by [44, 50]:

$$\varepsilon = 1 - \frac{\delta_0}{\delta} (1 - \varepsilon_0) \quad \text{Eq. (13)}$$

where δ_0 and ε_0 represent the initial thickness and porosity of the uncompressed porous medium, while δ and ε denote the final thickness and porosity of the compressed sample, respectively.

2.3.5. Validation

Several actions have been taken to validate the experimental method. Firstly, the binary, bulk diffusion coefficient D_b of oxygen in nitrogen ($\text{O}_2\text{-N}_2$) was reproduced by performing diffusion measurements without a sample in the holder. To ensure that the sample holder maintained its seal at different thicknesses, and to ensure that the end conditions were

constant at all thicknesses, the open air binary diffusion measurements were performed with shims ranging from 254 μm to 102 μm . The results for the bulk diffusion coefficient of O_2 in air at various shim thicknesses are illustrated in Figure 7. The average deviation of the measured from the accepted value, indicated by the solid line, is 1%.

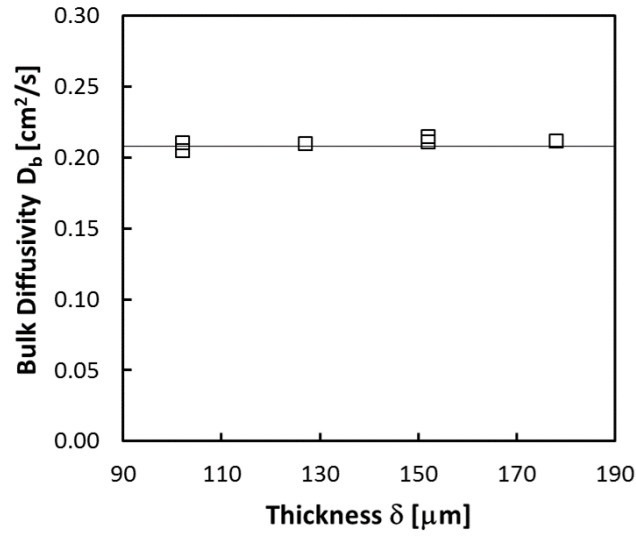


Figure 7: Bulk diffusion coefficient D_b of oxygen in nitrogen at various shim thicknesses δ .

The assumption of constant oxygen composition at the ends of the holder is perhaps the most questionable, given that oxygen will be depleted from the ends as it diffuses into the sample. This was investigated by performing experiments with the oxygen sensor placed at the end of the holder, and it was found that that the oxygen concentration was indeed constant at 20.9% for the entire duration of the experiment. Clearly, replenishment of the O_2 at the sample's ends from the surrounding air was much faster than its rate of diffusion into the sample. Potential convection into the sample chamber was ruled out by performing diffusion measurements with the holder placed inside a desiccator, providing a convection-free environment. These tests proved to have no effect on the resulting diffusion coefficient, indicating that convection effects were negligible.

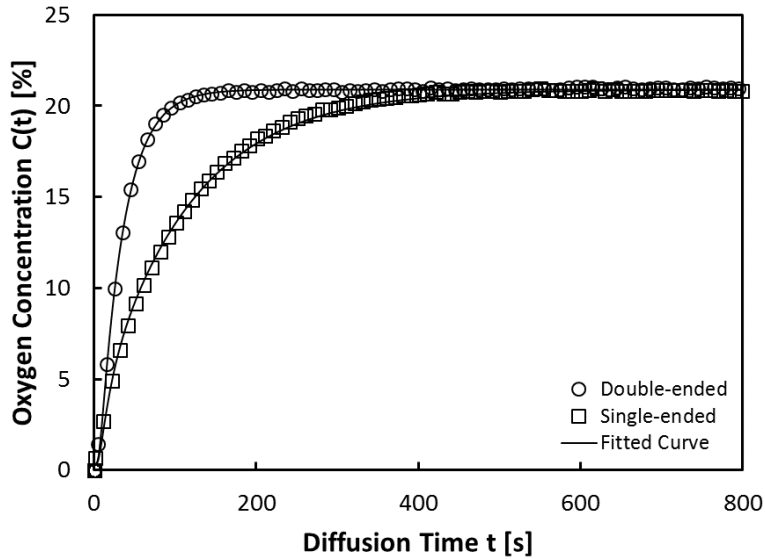


Figure 8: Oxygen concentration vs. diffusion time curves of single-ended vs. double-ended open air diffusion.

Finally, tests were performed with only one end of the holder open to air, while the other end was sealed. This effectively doubled the domain size and moved the sensor location away from the no flux position (the center in the dual ended arrangement). After adjusting the l and z parameter in Eq. (10) to this new geometry, the identical bulk diffusion coefficient is obtained as determined by the double-ended experiment. The recorded oxygen concentration for the single-ended and the double-ended measurements—along with the fitted curves—are illustrated in Figure 8. It was also checked that the sealing material was impervious to air by blocking both ends and confirming that the oxygen concentration did not increase over time.

2.4. Results and Discussion

Figure 9(left) shows the normalized effective diffusion coefficient D' of 24AA and 25AA as a function of compressed porosity. The normalized effective diffusivity D' decreases rapidly with decreasing porosities. The impact of compression is seen more clearly in Figure 9(right) where the experimental data is plotted directly as tortuosity vs. porosity. The value of tortuosity is slightly above 1 for the uncompressed materials, but rises continuously, approaching a value of 4 as the material is compressed to 50% porosity. The

25AA GDL shows slightly higher diffusivities than 24AA, but both data sets follow a very similar trend due to their similar morphology and fiber binder material, as can be judged from the SEM images presented by Flückiger et al [44]. The 24AA material appears to have slightly more binder, which is confirmed by its lower uncompressed porosity compared to 25AA (0.86 vs. 0.89).

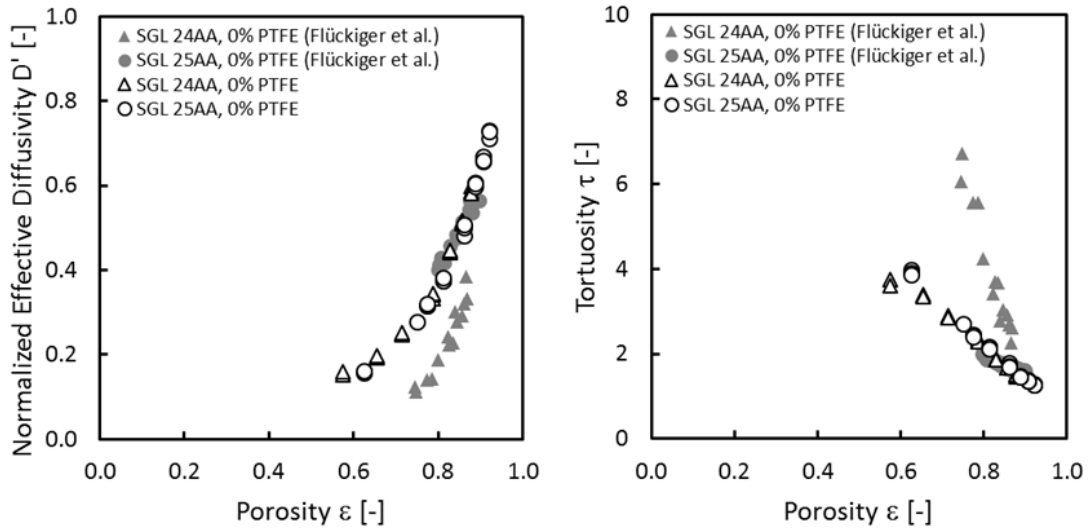


Figure 9: Normalized effective diffusivity D' vs. porosity ϵ and tortuosity τ vs. porosity ϵ of untreated SGL 24AA and SGL 25AA.

Also shown in Figure 11 are the data reported by Flückiger et al. for the same two materials [44]. The results for 25AA are in good agreement with the present data, however, 24AA results differ substantially. Upon closer consideration, it is somewhat surprising that Flückiger et al. [44] observed such high tortuosity for 24AA compared to 25AA, since the two materials are morphologically similar. To investigate whether the slight differences between the 4th and 5th generation materials could explain the significantly different diffusion behavior, tests were performed on 34AA and 35AA samples, which are identical to the 20 series materials in all respects, except slightly thicker. The results in Figure 10 show a similar trend as observed for the 20 series materials, with the 34AA having a slightly lower normalized effective diffusivity than the 35AA sample. This seems to suggest

that the large difference between 24AA and 25AA reported by Flückiger et al. [44] may be anomalous, although this issue will be revisited below in conjunction with PTFE addition. It must be pointed out that although the 34AA and 35AA materials behave similarly to each other, their tortuosity increases more rapidly than the 24AA and 25AA samples. Therefore, comparisons between series might not be so straightforward. The different thicknesses of the 20 and 30 series materials presumably lead to different strain behavior when they are compressed. For instance, the thinner 20 series materials might become damaged and cracked during compression, while the thicker 30 series could absorb larger strains. It has been shown by Fishman et al. [51] that supposedly identical materials with different thicknesses seem to be manufactured differently and do not necessarily have the same pore structure, which could also explain the differences seen between the 20 and 30 series materials in this study.

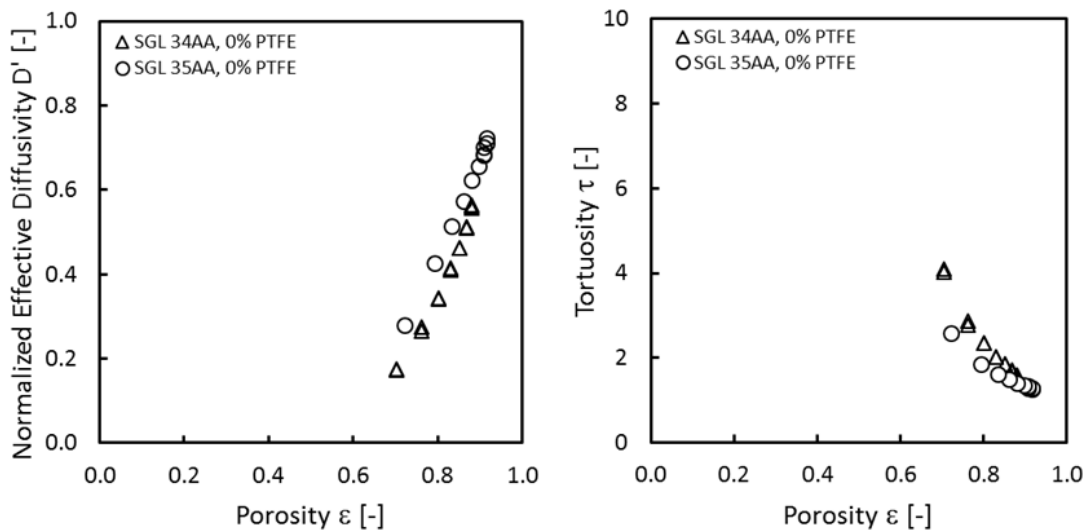


Figure 10: Normalized effective diffusivity D' vs. porosity ϵ and tortuosity τ vs. porosity ϵ of untreated SGL 34AA and SGL 35AA.

PTFE is typically added to GDL materials to increase their hydrophobicity and improve the water management in running fuel cells. This additional material certainly fills void space and reduces porosity, but may also block pores and increase the tortuosity depending how it is distributed. Figure 9 compares the D' vs. ϵ behavior of 24AA and 24DA. 24DA has a

lower initial porosity than 24AA due to the addition of 20 wt-% PTFE partially filling the pore space. Uncompressed, 24AA and 24DA show comparable effective diffusivities, but with increasing compression, the effective diffusivity of 24DA decreases more rapidly, compared to its untreated counterpart. This is very clearly illustrated in Figure 11(right), which shows the tortuosity of the two materials diverging strongly. This is a very interesting finding, since it suggests that PTFE does not simply reduce porosity, but actually alters the topology of the pore space. Upon compression, the PTFE inclusions apparently impinge the pore space and lead to higher tortuosity.

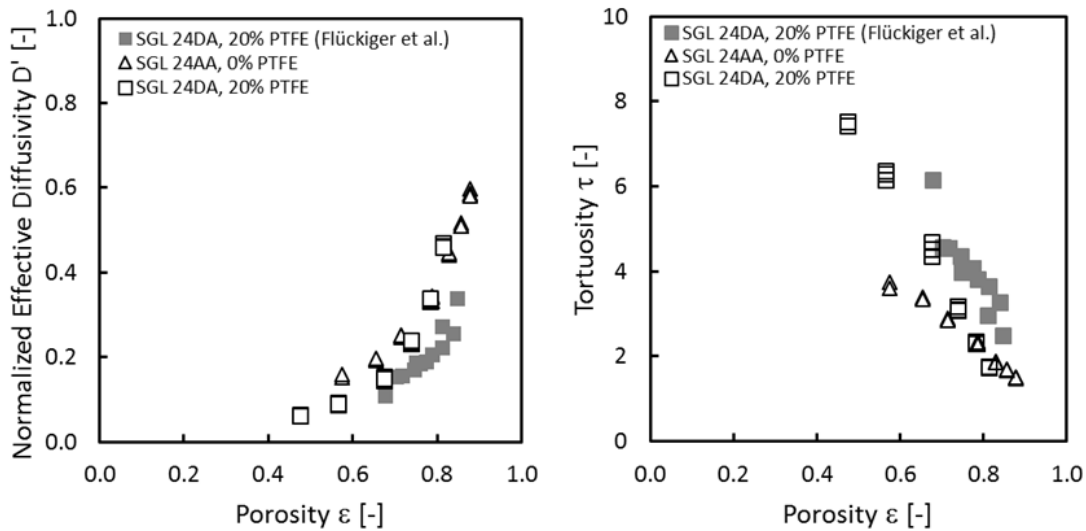


Figure 11: Normalized effective diffusivity D' vs. porosity ε and tortuosity τ vs. porosity ε of untreated SGL 24AA and PTFE treated SGL 24DA.

In contrast to the present results, the data of Flückiger et al. [44] indicate that 24AA and 24DA behave very similarly. In the preceding discussion, it was reasoned that their results for 24AA gave anomalously high tortuosity, given how little it differed from 25AA which has a similar morphology. The same reasoning, however, could also be used to argue that the present results for 24AA give an anomalously *low* tortuosity, given that 24AA and 24DA also have similar morphology and assuming that PTFE addition does not change the pore structure substantially. Therefore, it is not obvious whether the addition of PTFE (24AA vs. 24DA) or the presence of additional binder (25AA vs. 24AA) would have more

impact on the tortuosity. This dilemma could be solved by testing 25DA to determine if it differs significantly from 25AA, but this material was not available for testing. The deviations between these results could also be due at least in part to the variability in the materials. The present work aimed to develop and validate a viable alternative technique, thus, exploring the manufacturing variability is beyond its scope. Nonetheless, this would seem like a prudent study to perform in the near future.

2.5. Conclusions

A straightforward and cost-effective experimental technique to measure the IP effective diffusivity of single layers of thin porous materials such as GDLs for PEMFCs has been developed and validated. It was shown that this method could accurately reproduce the bulk diffusion coefficient of oxygen in nitrogen. It was also demonstrated that this value could be reproduced with one or both ends of the holder open, and over a range of plate spacing. The ability to reproduce the open-air diffusion coefficients in a variety of configurations indicates the robustness of this approach, and that the holder was leak proof, convective effects were negligible, boundary conditions were maintained, and the mathematical model was suitable.

To validate the measurements of effective diffusivity in porous materials, samples for which existing literature data was available [44] were tested. In general, the present results agreed very well with the literature values, with only one exception. The present results showed that the impact of PTFE addition had a stronger impact on tortuosity than differences in binder which are presumably more subtle. By contrast, the results of Flückiger et al. [44] showed very large differences between materials that had different binder arrangements, but saw little change with PTFE addition. Insufficient data was available to make conclusive comparisons. In any event, the close match between the present results and those of Flückiger et al. [44] were highly encouraging, and suggested that the present method is an equally accurate, yet far simpler approach for measuring effective diffusivity. Future work will focus on quantifying the impact of PTFE addition, the

effect of sample thickness for otherwise identical materials, and the importance of fiber morphology on tortuosity.

2.6. Acknowledgements

The funding provided by the Automotive Fuel Cell Cooperation (AFCC) and the Natural Sciences and Engineering Research Council (NSERC) of Canada is greatly appreciated. The authors also wish to thank SGL Group for donating GDL sample materials. The authors are grateful to Marios Ioannidis and Jörg Kleeman for valuable discussions on the interpretation of our results.

Chapter 3: In-plane effective diffusivity of gas diffusion layers for PEMFCs

Preface

In the first submitted manuscript to the *International Journal of Heat and Mass Transfer* and contained in Chapter 2:, a novel experimental technique was developed for the fast, accurate, and straight-forward determination of in-plane effective diffusion coefficients of thin, porous materials, specifically of gas diffusion layers [1]. The experimental method was validated through several experimental and theoretical means and results obtained for conventional gas diffusion layers were compared with literature. In the following chapter, the above established technique is applied to measure the effective diffusion coefficients of several commercial GDLs, namely materials manufactured by Toray, SGL, and Freudenberg. Furthermore, the effective diffusivity was measured as a function of compression in order to determine the impact of compressive load on the effective diffusivity. Prior to the diffusion measurements, the physical properties including thickness, bulk and skeletal density, areal weight, solid fraction and most importantly, the porosity of said porous media were characterized through appliance of Archimedes' principle, as reliable thickness and porosity data was scarce. The results and analysis of this study, authored by Rinat Rashapov, Jonathan Unno, and Jeff T. Gostick, were submitted and accepted to the *Journal of The Electrochemical Society* [3]. Due to length requirements, the study was not further elaborated in this thesis. However, the obtained thickness and porosity results were used for the determination of the effective diffusivities of above mentioned materials. Chapter 3: contains the manuscript, authored by Rinat Rashapov and Jeff T. Gostick, and submitted to *Transport in Porous Media* [2]. The study investigates the impact of compression, PTFE addition, binder, and different morphologies on the in-plane effective diffusion coefficient of various GDLs. It can therefore be regarded as a continuation of the previous chapter.

3.1. Abstract

The in-plane effective diffusion coefficients in gas diffusion layers typically used in fuel cell electrodes were measured as a function of compression and hydrophobic polymer loading. This method was based on the transient diffusion of oxygen from air into an initially nitrogen purged porous sample and has proven to be accurate, fast, and straight-forward. As anticipated, with higher compressions and higher PTFE loadings, effective diffusivity decreased, as a result of less pores space available for transport and because tortuosity increased. When plotted against compressed porosity, the effective diffusivity of untreated and treated materials for a given type of sample collapsed on top of each other, despite the simultaneous impact of PTFE-loading and compression. It was possible to distinguish between the impact of PTFE and compression by plotting the data as tortuosity against compressed thickness. High compressions on the sample lead to irreversible damages to the fiber structure, resulting in decreased or unexpectedly low tortuosity. Finally, a percolation model was fitted through one of the tested materials and a reasonable agreement was observed for lower compression, but a fit to the entire data could not be achieved. This was attributed to fundamental structural changes occurring in the sample upon high compressions, an observation that helps to explain the general inability of theoretical tortuosity models to describe GDLs.

3.2. Introduction

Polymer electrolyte membrane fuel cells (PEMFCs) are the leading candidate to substitute conventional internal combustion engines in the near future, as they are only available power source that offers equivalent range and power density. A typical PEMFC converts stored hydrogen and oxygen from air to generate electricity, while producing only waste heat and pure water. A detailed description of PEMFC operation can be found in review articles [27, 28, 52] and textbooks [29, 30]. The main components of a PEMFC consist of two bipolar plates (BPs), two gas diffusion layers (GDLs), the central polymer electrolyte membrane, with catalyst layers (CLs) applied to both sides. Though PEMFCs can be 2-3 times more efficient than combustion engines, several challenges must still be overcome

before commercialization of PEMFCs for mobile applications, e.g. in the automotive industry, can be possible. Along with the development of a more cost-effective and efficient catalyst material for the electrochemical reaction, another major difficulty lies in the effective management of reactants and products inside the cell. Particularly at high current densities, mass transport becomes rate limiting, leading to concentration polarization and a decrease in cell voltage. This necessitates larger stacks to accommodate peak power requirements. Improving mass transfer therefore represents an opportunity to reduce overall system costs by facilitating smaller stacks.

Understanding the transport characteristics of the GDL is vital, as it supports most transport processes inside the fuel cell, such as reactant and product mass transfer, heat transfer, and electron conduction and thus plays a major role during fuel cell operation [53]. The 150-400 μm thin sheets are made from carbon fiber and exhibit high porosities ranging from 70-90%. The fibrous structure and morphology of several conventional GDLs can be seen in Figure 12. Due to the production of water vapor and partial condensation during fuel cell operation, GDLs are treated with a hydrophobic polymer such as PTFE to prevent water from wicking throughout the pore space. The addition of PTFE is necessary to limit the deleterious effect of water, but also causes mass transfer restrictions by partially filling the pore space. GDLs are also the only compliant item in the cell so they are mechanically compressed during stack assembly, upon swelling of the ionomer with water uptake, or during water freeze-thaw cycles. Mass transport through the GDL is more complex than simply assuming diffusion through an idealized stack of fibers. For instance, many of the established correlations for predicting diffusivity from basic structural information, such as the widely used Bruggeman equation [54], or the fibrous materials specific studies of Tomadakis and Sotirichos [55, 56], both substantially over-predict effective diffusivity in GDLs. Experimental determination of the effective diffusivity is therefore necessary. Furthermore, due to their fibrous mat structure, the effective diffusivity in the direction of fiber alignment, known as the in-plane (IP) direction is higher than in the through-plane (TP) direction, thus measurements must be made in both the

IP and TP directly to determine anisotropy and to properly characterize these materials [57].

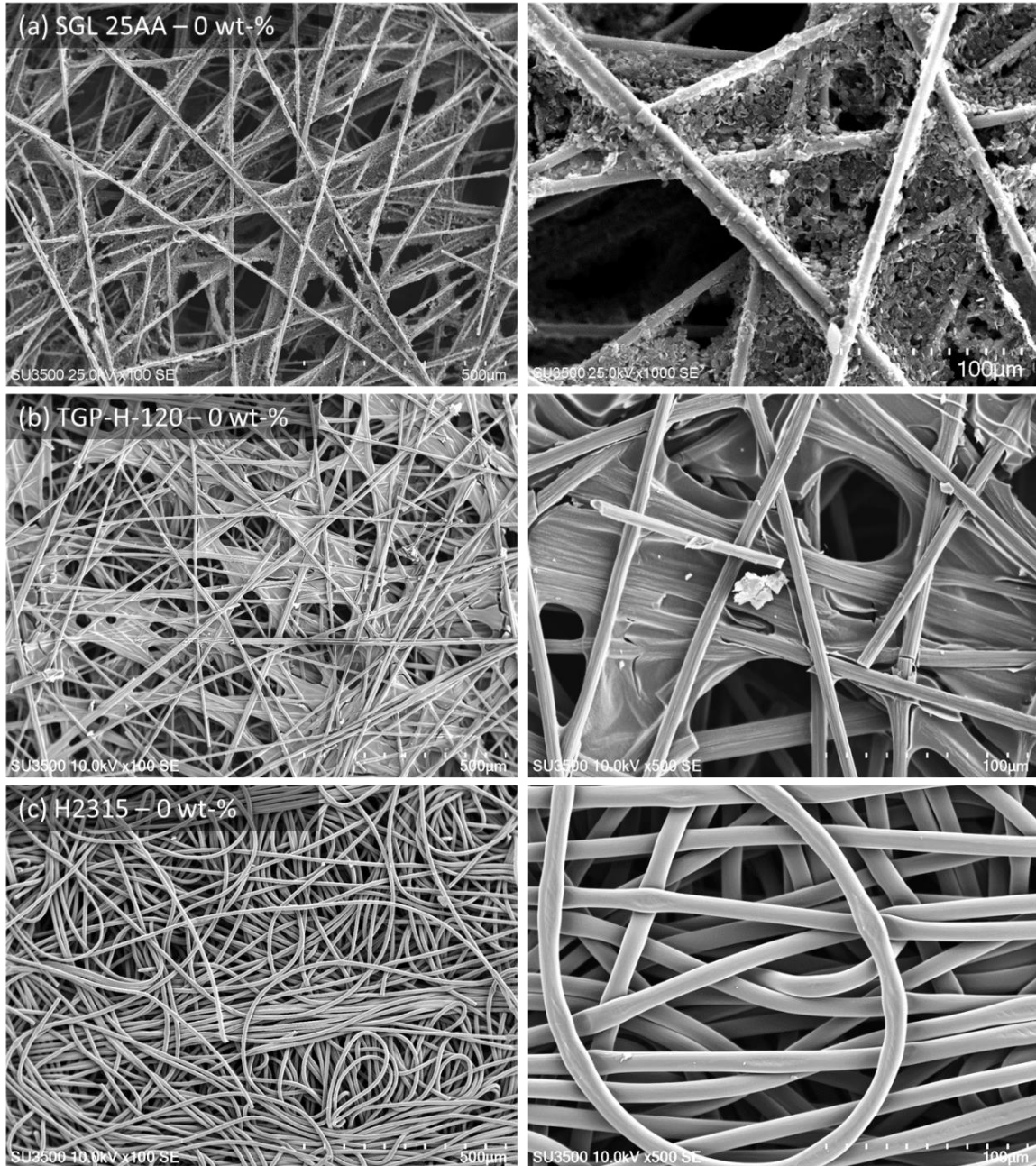


Figure 12: SEM micrographs of untreated SGL 25AA, TGP-H-120, and Freudenberg H2315. Images on the right show a magnified view.

Most experimental studies focus on the effective diffusion of gasses in various GDLs in the

TP direction. This is sensible, since the reactant and product diffusion in a fuel cell is directed from the flow channels in the bipolar plates towards the CLs and vice versa, thus, occurring in the TP direction. Astrath et al. [58] and Zamel et al. [37] adapted a Loschmidt method [36] to study the TP diffusion behavior of oxygen gas in nitrogen gas through TGP-H-120 Toray paper. Quick et al. [38] and LaManna et al. [39] created a humidity gradient in the porous sample, and determined the water vapour TP permeability and effective diffusivity of various GDLs. Baker et al. [43] applied a limiting current technique in a specialized single channel cell to measure the effective TP diffusivity of oxygen gas and water vapour through SGL and Toray materials. Utaka et al. [41, 59] developed a galvanic cell type oxygen sensor to measure the effective TP diffusivity of oxygen through a paper-type GDL. In order to determine the effective TP diffusivity of unsaturated and partially-saturated GDLs, Hwang and Weber [42] developed an electrochemical limiting-current technique in a fuel cell-type assembly, but using a hydrogen pump reaction.

Though less directly relevant to fuel cell power production, IP diffusion is nonetheless essential to fuel cell operation, as reactants must also be dispersed to regions of the CL located under the ribs of the bipolar plate to fully utilize the catalyst sites. To the best of the authors' knowledge, only Kramer et al. [34] have developed an experimental technique which allows for the determination of effective diffusivities in the IP direction. They refer to their method as electrochemical diffusimetry, which exploits the relationship between Ohm's and Fick's law. In their method a GDL is saturated with an electrolyte, and through electrochemical impedance spectroscopy, the effective ionic conductivity and therefore the effective diffusivity is experimentally determined. In a previous study [1], a novel experimental technique for the direct measurement of effective IP diffusivity of individual GDLs was developed and validated. The method was based on measuring the time-dependent oxygen concentration at a fixed position inside the sample and fitting for the diffusion coefficient. Compared to the electrochemical diffusimetry technique mentioned above, this method was fast and technically much more straightforward to apply. In the present study, this experimental technique was applied to measure the IP

effective diffusivity of a wide variety of untreated and PTFE-treated SGL, Toray, and Freudenberg materials. The impact of PTFE loading and compressed thickness on the diffusivity and tortuosity was determined, and a theoretical model was fitted to the experimental data to compare results.

3.3. Experimental

3.3.1. Method

The experimental method used in this study for measuring the effective diffusion coefficient in the IP direction of various GDLs was developed and validated in a previous study [1]. The technique has proven to be simple, fast, and accurate, and allows the investigation of compression on effective diffusivity of individual GDL samples over a wide range of compressions. Firstly, the GDL sample was cut from a larger sheet into 3" x 1/8" strips and its thickness was measured using a micrometer before it was placed centrally between two 1" thick stainless steel plates as illustrated in the experimental setup shown in Figure 13. The compression of the sample was controlled by stainless steel shims of known thickness ($\pm 1\mu\text{m}$) placed between the two sample holder plates. Upon tightening and sealing the apparatus, only the ends of the samples were exposed to atmospheric conditions. Subsequently, the porous sample was flushed with nitrogen gas for approximately one minute to set a zero oxygen initial condition throughout the porous sample. Once flushing was stopped, atmospheric oxygen immediately started to diffuse through both ends until the concentration gradient inside the GDL dissipated. An oxygen sensor (OceanOptics FOXY-NeoFox[®]), placed at a fixed position inside the sample, recorded the increase in oxygen concentration as a function of time. Once the measurement was completed, the spacer shims were replaced by thinner ones and the apparatus was sealed again, thus, increasing the compression of the sample. Depending on the uncompressed sample thickness and its PTFE loading, up to nine different compressions were applied to the materials.

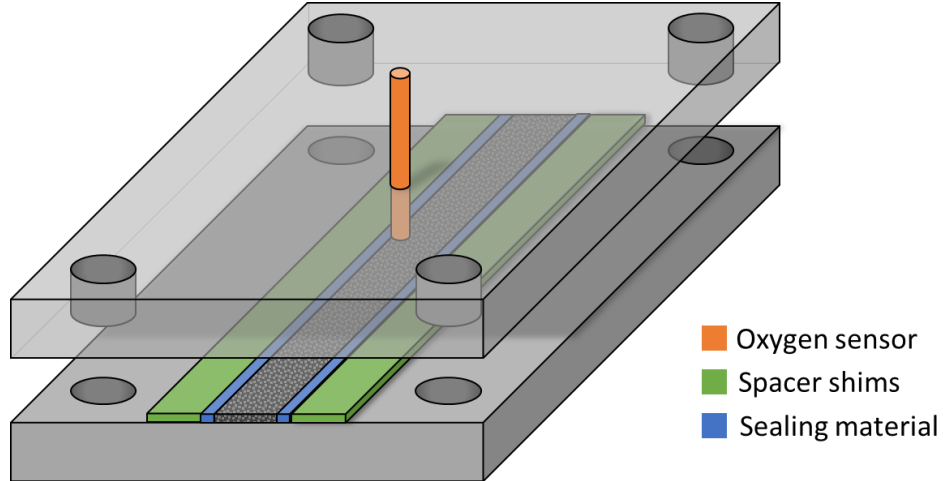


Figure 13: Schematic of the experimental setup to measure the effective diffusivities of GDLs.

Measurement of effective diffusivity, D_{eff} , in porous materials aims at providing diffusion coefficients for using in Fick's law that account for not only the relative molecular mobility (D_b), but also the impact of solid phase obstacles. Values of D_{eff} through a porous material are always lower than through open-space, since the solid obstacles both reduce the effective area for flux and also increase the average length of the diffusion pathways. Effective diffusivity is typically defined as:

$$D_{eff} = D_b \frac{\varepsilon}{\tau} \quad \text{Eq. (14)}$$

where ε is the porosity of the media ($\varepsilon < 1$) and τ is the tortuosity ($\tau > 1$), accounting for the increased path lengths of diffusion molecules around solid obstacles relative to the length of the domain [18-21]. Assuming the porosity is known through independent means [3], τ is essentially a fitting parameter to reconcile differences between D_b and measured values of D_{eff} .

In order to determine the effective diffusion coefficient, Fick's second law was solved analytically for one dimension [46]:

$$\frac{C(t) - C_0}{C_1 - C_0} = \sum_{n=0}^{\infty} (-1)^n \operatorname{erfc} \frac{(2n+1)l - z}{2\sqrt{Dt}} + \sum_{n=0}^{\infty} (-1)^n \operatorname{erfc} \frac{(2n+1)l + z}{2\sqrt{Dt}} \quad \text{Eq. (15)}$$

where $C(t)$ is the measured concentration at position z , C_0 and C_1 are the initial (0%) and final (20.9%) oxygen concentration, respectively, l is the domain length, and D is the diffusion coefficient. The effective diffusion coefficient is determined for each compression from fitting Eq. (10) to the experimentally measured diffusion curves. A detailed data analysis can be found in a previous article [1].

3.3.2. Thickness and Porosity

Prior to the diffusion measurements, the sample specific average thickness δ_0 of each GDL was determined across ten different locations using a Mitutoyo micrometer (readability 1 μm). Buoyancy measurements in silicone oil, as reported in [3], were performed in order to obtain the uncompressed porosity, ε_0 . The bulk volume can be determined by measuring the diameter of the circular sample, d , and the uncompressed thickness, δ_0 . The results obtained for thickness, areal weight, bulk density, skeletal density, and porosity of various SGL, Toray, and Freudenberg GDLs were reported in a previous study [3].

As compression on the porous sample increases, its porosity drops, since fibers are forced closer to each other and thus, a smaller fraction of void space is available for diffusive mass transport. The compressed porosity, ε , can be estimated from:

$$\varepsilon = 1 - \frac{\delta_0}{\delta} (1 - \varepsilon_0) \quad \text{Eq. (16)}$$

where ε_0 represents the uncompressed porosity, and δ_0 and δ the uncompressed and compressed thickness of the sample, respectively. The measured effective diffusivity is normalized by relating it to the measured bulk diffusivity, D_b , of nitrogen in oxygen gas with no porous sample present.

3.3.3. Materials

Table 2: Thickness, Porosity, and PTFE Loadings of tested GDL Materials

Manufacturer	Material	PTFE	Corrected PTFE	Thickness	Porosity
		[wt-%]	[wt-%]	[μm]	[%]
SGL	24AA	0	0	181	85.4
SGL	24BA	5	1	198	85.1
SGL	24CA	10	14	181	82.1
SGL	24DA	20	28	184	79.0
SGL	24EA	30	41	178	74.8
SGL	25AA	0	0	178	88.4
SGL	25BA	5	3	177	88.2
SGL	34AA	0	0	252	84.1
SGL	34BA	5	8	280	82.7
SGL	34CA	10	18	251	79.8
SGL	34DA	20	25	268	78.5
SGL	34EA	30	34	264	75.4
SGL	35AA	0	0	264	88.4
SGL	35BA	5	-4	278	89.0
Toray	TGP-H-060	0	0	183	74.4
Toray	TGP-H-060	5	2	187	73.9
Toray	TGP-H-060	10	0	200	73.8
Toray	TGP-H-060	20	28	187	66.8
Toray	TGP-H-060	40	12	188	70.8
Toray	TGP-H-060	60	55	183	44.3
Toray	TGP-H-090	0	0	296	74.5
Toray	TGP-H-090	5	9	268	71.9
Toray	TGP-H-090	10	9	286	72.2
Toray	TGP-H-090	20	24	291	67.3
Toray	TGP-H-090	40	42	286	58.3
Toray	TGP-H-090	60	54	292	50.1
Toray	TGP-H-120	0	0	367	76.2
Toray	TGP-H-120	5	10	363	74.6
Toray	TGP-H-120	10	14	368	73.1
Toray	TGP-H-120	20	20	374	69.5
Toray	TGP-H-120	40	43	357	60.7
Toray	TGP-H-120	60	61	348	43.9
Freudenberg	H2315 T0	0	0	132	68.7
Freudenberg	H2315 T10A	10	4	183	68.2
Freudenberg	H2315 T20A	20	19	186	62.5
Freudenberg	H2315 T40A	40	35	175	54.7

Table 2 summarizes the materials and their specifications used for effective diffusivity determination in this study and includes untreated and PTFE-treated GDLs manufactured by SGL, Toray, and Freudenberg. The PTFE content of the tested GDLs ranged from 0-60 wt-% for Toray, 0-30 wt-% for SGL, and 0-40 wt-% for Freudenberg materials. Only untreated

and 5 wt-% PTFE treated SGL 25 and SGL 35 GDLs were available in this study. However, it has been shown that reported PTFE-loadings do not always comply with the actual amount of PTFE found in GDLs [3]. Table 2 includes the corrected PTFE content obtained by weighing the treated sample, and assuming any differences in bulk density relative to an untreated sample were due to the added mass of PTFE. In this study, only dry GDLs without a MPL were considered.

3.4. Results and Discussion

The three materials measured in this study differ in subtle ways that provide an interesting basis for comparison. The Toray materials and SGL materials both consist of linear fibers stacked into a highly anisotropic mat, while the Freudenberg materials contain curved, entangled fibers that are expected to be at somewhat more isotropic. Furthermore, as can be seen from SEM images shown in Figure 12, the SGL materials are filled with a porous binder as a result of the manufacturing process, while the binder in the Toray materials is relatively smooth and non-porous. The SGL samples have a much higher uncompressed porosity compared to Toray, 85-88% compared to 75% for untreated materials. It is likely that the Toray and SGL materials have different numbers of fibers per unit volume which accounts for some of this difference. Inspection of Figure 12, however, suggests the materials appear quite similar in this regard, which suggests that the binder in the SGL materials is quite porous. Additionally, Figure 12 displays that Freudenberg H2315 samples are completely binder-free.

Since the SGL 24/34, SGL 25/35, and the Toray materials differ only in thickness, while all other specifications such as porosity, skeletal density, morphology, and binder material are almost identical, only one representative sample from each class of materials was included in the following discussion: SGL 24, SGL 25, TGP-H-120, and H2315. Experimental data for all GDLs listed in Table 2 is included in the Appendix in Figure 21 through Figure 23.

Thickness of the uncompressed material was not investigated as a parameter since in principle diffusivity is independent of domain size (i.e. thickness is not required in Eq. (10)). There are some reports that materials of different thickness have slightly different internal structures, seen as through-plane porosity profiles [60], but the impact of this was not observed in the present data.

3.4.1. Effective Diffusivity

Figure 14 illustrates the measured normalized effective diffusivity of SGL 24, SGL 25, TGP-H-120, and H2315 as a function of compressed porosity. As anticipated, increasing compression results in a decrease in effective diffusivity, due to the reduction in porosity, and possibly also due to increased diffusion pathway lengths. The most immediately clear observation is that the diffusivity trends of untreated and treated materials of the same type essentially collapse on top of each other. Both PTFE addition and compression reduce the baseline porosity of GDLs and therefore effectively reduce pore space available for transport [61, 62]. The results in Figure 14 show that these two variables have essentially the same effect on the overall effective diffusivity in the materials, although the relative contributions of these two factors are evaluated in more detail later on.

Despite having lower uncompressed porosity, the TGP-H-120 samples exhibit higher effective diffusivities than SGL 24 at the same compressed porosity. This result contradicts the general premise that higher porosity materials should exhibit higher diffusivity. Given that these two materials have similar fibrous structures, the differences are likely due to the binder. This suggests that the pores in the binder of the SGL samples do not contribute significantly to the overall effective diffusion, meaning they are not well connected, or they are highly constricted. This has important repercussions for transport modeling, since it suggests that the total measured porosity of SGL materials does not represent the amount of useful pore space that actually contributes to transport. Any correlations that rely on values of the porosity, such as the Carman-Kozeny or Bruggemen correlations, would therefore result in over-predictions using SGL's bulk porosity. It is difficult to

determine precisely how much of the pore space in the SGL materials resides in the binder (without tomography or porosimetry techniques), and even more difficult to assess the diffusivity in the binder. The SGL 25 series materials have an even higher uncompressed porosity (>88%) compared to Toray, which can be visually observed with SEM [3]. The differences in binder are apparently quite important, since the SGL 25 materials have a much better diffusivity, matching the TGP-H-120 samples at a compressed porosity of 60%. In addition to the binder, differences in diffusivity between the various GDLs may also be due to different numbers of fibers per unit volume.

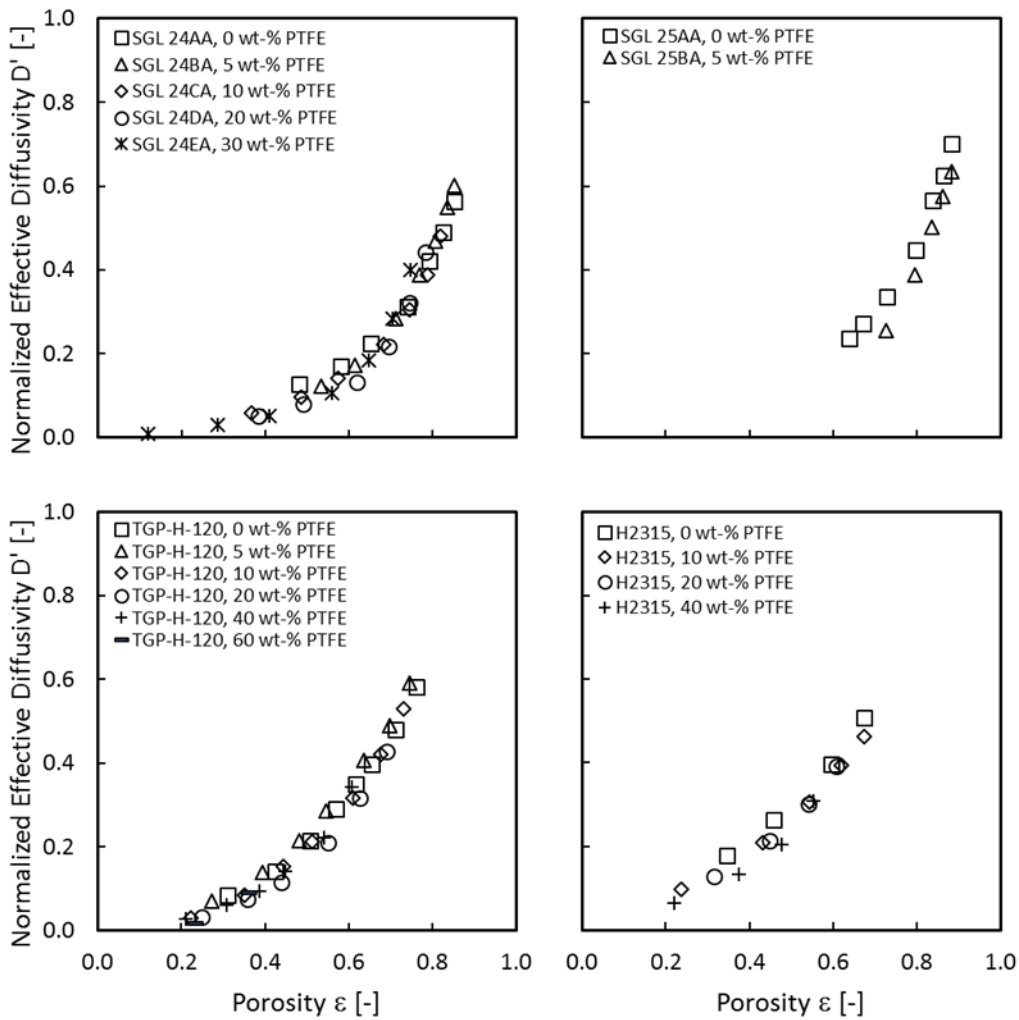


Figure 14: Normalized effective diffusivity D' vs. compressed porosity ε of untreated and treated SGL 24, SGL 25, TGP-H-120 and Freudenberg H2315.

Figure 12 shows a SEM image of untreated Freudenberg H2315 at two magnifications. Both micrographs illustrate a substantial difference in fiber structure and morphology compared to linear fibers seen in SGL and Toray carbon papers. The entangled nature of the fibers in this material allows for a higher packing density, and consequently, the H2315 samples exhibit lower uncompressed porosities compared to Toray and SGL samples. Figure 14 shows that the effective diffusivities of H2315 are substantially higher than for the linear fiber materials. Not only is this result unexpected on the basis of the lower porosity of the H2315 materials, but the entangled fibers would presumably be somewhat more isotropic than the linear fibers, suggesting that the IP diffusivity is expected to be even lower than the other materials (i.e. it should behave more like through-plane diffusion). The only plausible explanation for this contradictory behavior is that the H2315 materials contain no visible binder, as can be seen in Figure 12(c). If correct, this explanation suggest that the presence of binder is quite detrimental to pore-space transport processes.

3.4.2. Tortuosity

As indicated in Figure 14, measured effective diffusivities for a given sample as a function of compression are almost coincident, regardless of how much PTFE was added. This suggests that porosity reduction by compression has the same overall impact on effective diffusivity as porosity reduction due the addition of extra PTFE. The results in Figure 14 are somewhat convoluted however, since porosity is a factor on both axes, as normalized effective diffusivity is equal to ε/τ according to Eq. (14). This is further confounded by the fact that τ is generally found to be a function of ε , such as stated in the Bruggeman relationship [54]. Rearrangement of Eq. (14) allows the determination τ as a function of ε from measured diffusivity values as shown in Figure 15. When plotted in this form, it becomes immediately apparent that samples with different PTFE loadings do indeed exhibit different behavior upon compression, as samples with higher PTFE loadings show a much steeper increase in τ and the curves begin to separate according to their respective PTFE contents. Evidently, the addition of PTFE has a significant impact on

effective gas diffusion and makes the porous medium more tortuous. This trend was not clearly visible in Figure 14, since according to Eq. (14), low values of ε are divided by large values of τ , obscuring the relative contributions of the two factors.

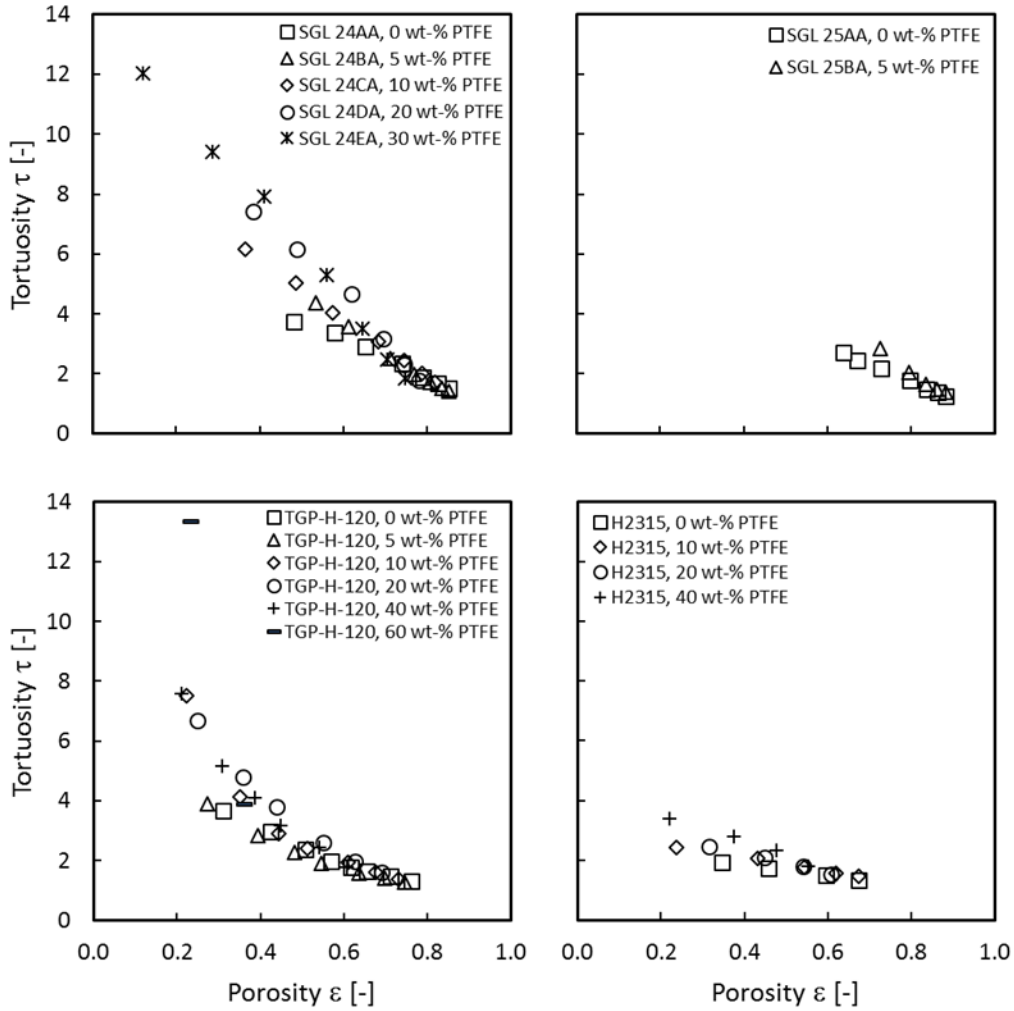


Figure 15: Tortuosity τ vs. compressed porosity ε of untreated and treated SGL 24, SGL 25, TGP-H-120 and Freudenberg H2315.

By definition, the tortuosity at 100% porosity is equal to 1, as the diffusion path is not hindered by any solid material and tortuosity increases with the decrease of void space fraction. Therefore with higher compressions, tortuosity of a porous sample is expected to increase steadily, and at very high compressions should rise infinitely as a porosity is

reduced to the percolation value, meaning that the void space is not connected and unavailable for mass transport. Though the results in Figure 15 show a steady increase in tortuosity with higher compressions, tortuosity generally does not rise towards infinity, but instead approaches a finite tortuosity value. This finding is consistent with the fact that at extremely high compressions, permanent damage and cracks are introduced into the brittle fibers and binder materials, thus supplying additional pathways for diffusion.

3.4.3. Thickness Ratio

Plotting tortuosity as a function of compressed porosity as done in Figure 15 revealed that samples with higher PTFE loadings clearly exhibited substantially increased in diffusion path length or tortuosity. The porosity values on the x-axis of Figure 14 and Figure 15 represent the combined impact of PTFE addition and compression. To fully differentiate these two factors, it is useful to plot tortuosity as a function of sample compression ratio, δ_0/δ , as shown in Figure 16. The justification for this normalization scheme is illustrated schematically in Figure 17, which considers two samples of the same type, one untreated and one treated with PTFE. Being of the same base-type means both GDLs should have the same initial thickness, thus differences in the tortuosity of these two samples in an uncompressed state can be entirely attributed to the presence of PTFE (case A vs. C). Similarly, when these two samples are compressed the same fixed amount, they will both display an increase in tortuosity, but the *difference* between the samples will still be due to the presence of PTFE (case B vs. D). When plotted against porosity, these changes in tortuosity are obscured by horizontal shifts, but when plotted against compression ratio, the impact of PTFE manifests itself as a parametric effect resulting in a distinct data series for each sample. Plotting the data in this way provides a powerful means of simultaneously evaluating the separate impacts of PTFE and compression.

Figure 16 shows the calculated tortuosity of SGL 24, SGL 25, TGP-H-120, and H2315 as a function of thickness ratio. The effect of PTFE on the tortuosity is clearly apparent and an increase in PTFE content directly results in an increase in GDL tortuosity. Though only

slight differences in tortuosity are observed between GDLs treated with 0 and 5 wt-% PTFE, this trend unfolds more distinctly at higher PTFE loadings. For almost all materials, tortuosity increases approximately linearly at low compression ratios. For higher PTFE loadings, tortuosity increases more rapidly particularly at higher compressions, as seen with TGP-H-120 treated with 60 wt-% PTFE. This suggests that when PTFE is present, the pore space collapses more quickly upon compression.

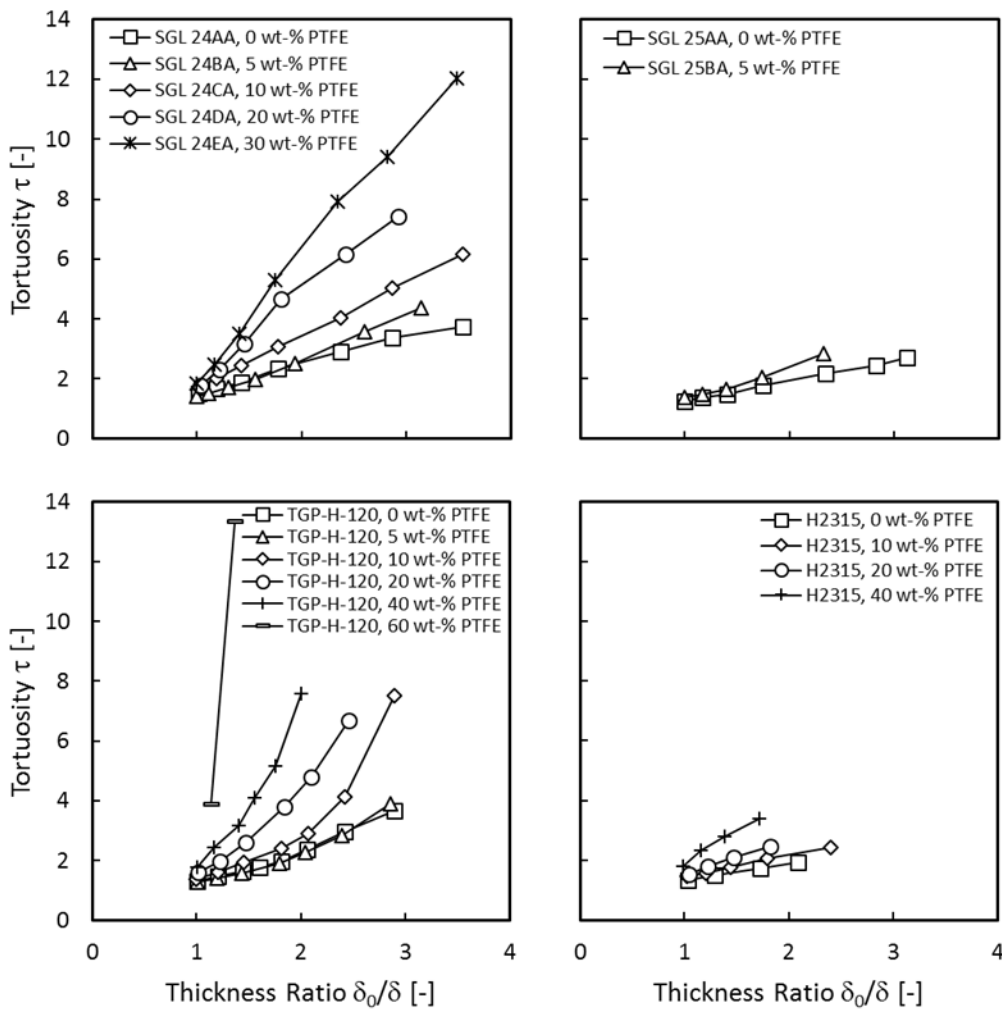


Figure 16: Tortuosity τ vs. thickness ratio δ_0/δ of untreated and treated SGL 24, SGL 25, TGP-H-120 and Freudenberg H2315. Lines through data points are to guide the eye only.

Freudenberg H2315 behaves differently with increasing compressions. It has already been

observed that H2315 exhibits surprisingly high effective diffusivity values, given its entangled and more isotropic fiber arrangement. According to Figure 16, it seems that the tortuosity of these materials is very low, and is not impacted significantly by compression. This can be rationalized by considering that the entangled fibers probably behave much differently upon compression than linearly stacked fibers. In the latter case, compression would directly reduce the size of openings between the fibers, while in the case of entangled fibers their displacement will be in random directions. The impact of PTFE addition on tortuosity is more in line with the other materials. For instance, both TGP-H-120 and Freudenberg H2315 treated with 20 wt-% PTFE have tortuosity values around 4 at a compression ratio of approximately 2.

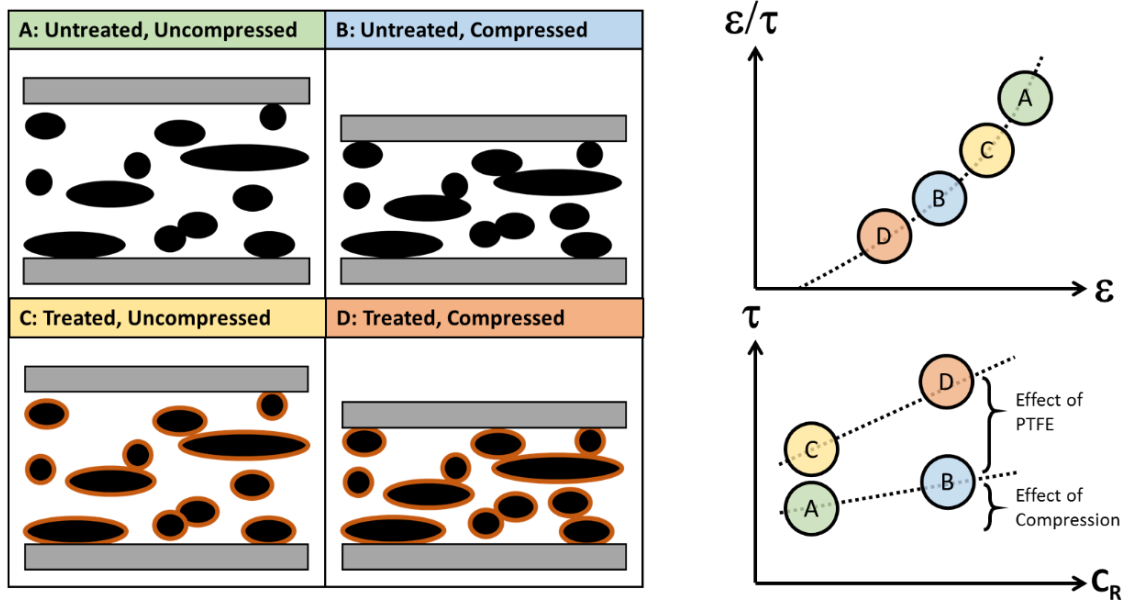


Figure 17: Schematic illustration comparing the impact of compression and PTFE loading for two different samples at two different compression ratios, C_R .

Another advantage of plotting the tortuosity against thickness ratio is that comparisons can be made between different materials at the same PTFE loading, regardless of their uncompressed porosity. This is useful for engineering decisions since the GDL compressed thickness is specified during cell assembly, therefore it is more valuable to compare

tortuosity as a function of thickness, rather than porosity. Figure 18(left) shows the tortuosity for all tested samples with no PTFE present. All GDL samples behave fairly similarly, with tortuosity varying from 1.5 to 4 of the whole range of compressions. One notable feature is that the SGL 25/35 series materials exhibit considerably lower tortuosities than the SGL 24/34 materials. Apparently, the newer generation of GDLs have improved mass transport characteristics, possibly due to less binder, or the pores in the binder contributing to mass transport. Some odd behavior is seen in the Toray samples, where the TGP-H-060 and TGP-H-120 samples agree quite well, while TGP-H-090 sample displays lower tortuosity. TGP-H-090 samples were obtained at later date than the other samples, resulting in differences in batches or lot numbers. When comparing samples at 20 wt-% PTFE in Figure 18(right), they again all behave similarly ranging between 2 and 8 as the thickness ratio varies from 1 to 3. The exception is the Freudenberg H2315 GDL, which demonstrates lower tortuosity. Perhaps this is due to the way PTFE agglomerates within the entangled fiber structure compared to the linear fiber materials. Here again TGP-H-090 material differs from TGP-H-060 and TGP-H-120, having lower tortuosities. Furthermore, Figure 18 does not include the SGL 25/35 series that compared so favorably at 0 wt-% PTFE, since these materials were not available with 20 wt-% PTFE. In summary, the fact that the tortuosity is fairly consistent between the various materials of the same PTFE loading regardless of compressed thickness means that differences in the overall observed effective diffusivity between samples is largely controlled by porosity and general solid phase structure.

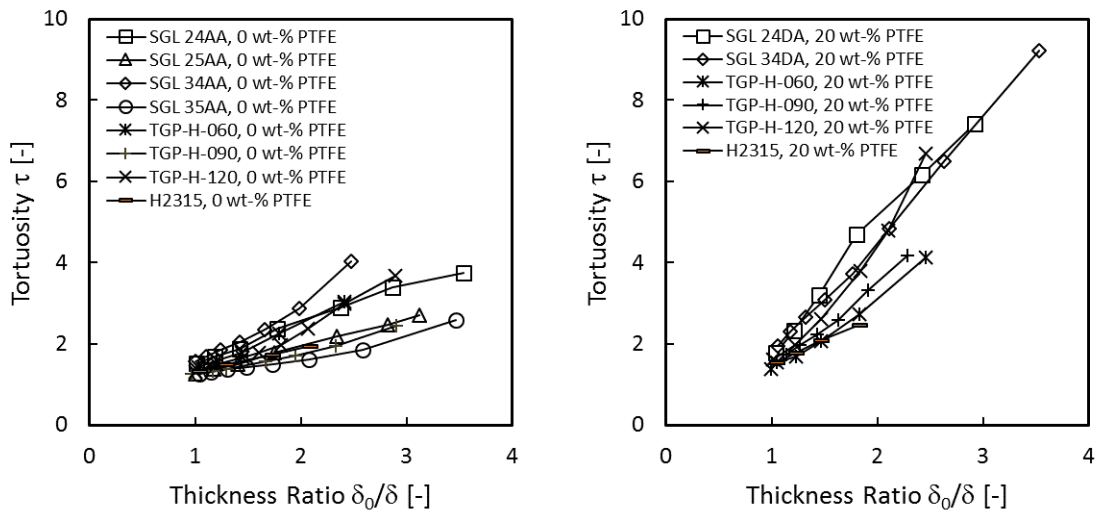


Figure 18: Measured tortuosity vs. thickness ratio of tested untreated (left) and 20 wt-% PTFE-treated (right) GDL materials.

3.4.4. Comparison with Percolation Theory

An attempt was made to fit the present data to an analytical model describing tortuosity as a function of porosity. Detailed reviews of tortuosity models can be found in literature [21, 63]. Bruggeman [54] derived a simple power law expression for estimating the effective conductivity and dielectric constant of a medium composed of only spheres: $\tau = \varepsilon^{-0.5}$. Due to the analogy between electric conduction and diffusion, this model also applies for describing diffusive mass transport. This equation is widely used in the fuel cell modeling literature and elsewhere, presumably due to its simplicity, though this expression does not predict accurate values for fibrous GDLs [44]. More specifically for fibrous media, Tomadakis and Sotichros [55] performed random walk simulations within domains filled with generated cylinders representing fibers, and estimated percolation properties as a function of fiber arrangement and packing density or porosity. Although based on fibers, their work still underestimates tortuosity, most likely because they did not account for binder or other filler materials in their idealized fiber structures. Moreover, the influence of porosity reduction was investigated by adding more fibers to the domain, a process which is not necessarily equivalent to compression. Das et al. [64] reviewed and evaluated diffusivity models with the aim of describing diffusivity in fuel cell electrode

materials, including GDLs. They adapted a percolation-type model developed by Hashin and Shtrikman [65] and derived a formulation for the estimation of effective transport properties in both TP and IP directions, which is algebraically equivalent to the classic model by Neale and Nader [66] and actually predicts lower tortuosity than the Bruggeman [54] correlation. Shou et al. [63] performed numerical simulations on randomly aligned fibers and evaluated a number of fiber-specific models for describing effective diffusivity in TP as well as in IP direction, but similar to Tomadakis and Sotichros [55], their results were based on idealized structures and under-predicts tortuosity. In general, all theoretical models are based on simplified geometries such as randomly aligned spheres or cylindrical and therefore cannot capture the complex fibrous structure of a real GDL, including non-idealities such as binder, PTFE, and damage in its morphology. The lack of a suitable functional form that can describe the behavior of GDLs over the entire range of porosity is highlighted by the work of Zamel et al. [67], who resorted to a purely empirical correlation in order to describe experimental GDL data.

The present data provide an excellent opportunity to further investigate correlations to describe tortuosity in GDLs, at least in the IP direction. The most basic functional form available is the following general percolation equation [68]:

$$\tau = \left(\frac{1 - \varepsilon_p}{\varepsilon - \varepsilon_p} \right)^\alpha \quad \text{Eq. (17)}$$

where ε_p represents the percolation threshold, and α is a fitting parameter. Tomadakis and Sotichros [55] used this form to describe their theoretical results, and reported ε_p as 0.11, and α as 0.785 for random 2D fibers, with slight differences for different fiber alignments. In this study, an attempt was made to determine a value or values of α that could describe the entire data set for the TGP-H-120 material, which was chosen since its linear fibers and non-porous binder most closely represent the ideal materials used in modeling studies. The previously established value of 0.11 for ε_p was adopted here, as no

clear percolation threshold could be observed from the data shown in Figure 14, presumably as a result of fiber breakage, effectively decreasing tortuosity. Therefore, Eq. (17) required fitting only α as a single parameter.

Figure 19(left) shows an attempt to fit a line through all points for each PTFE loading using a single value of α , plotted as tortuosity as a function of thickness ratio. It was not possible to fit the entire range of compressions. In general, an excellent fit was obtained at low compressions, however, as compressions increased, the experimental data always tended to fall below the model curves. This tendency agrees with the explanation of brittle carbon fibers and binder material being crushed and broken at high compression ratios. Physical damage and destruction of the solid phase ultimately alters the physical structure, hence, a single value of α should *not* be expected. It seems that the inability of existing theoretical models to fit the experimental data is not due to a problem with the models, but rather to fundamental changes in the morphology of the material as it is compressed and damaged.

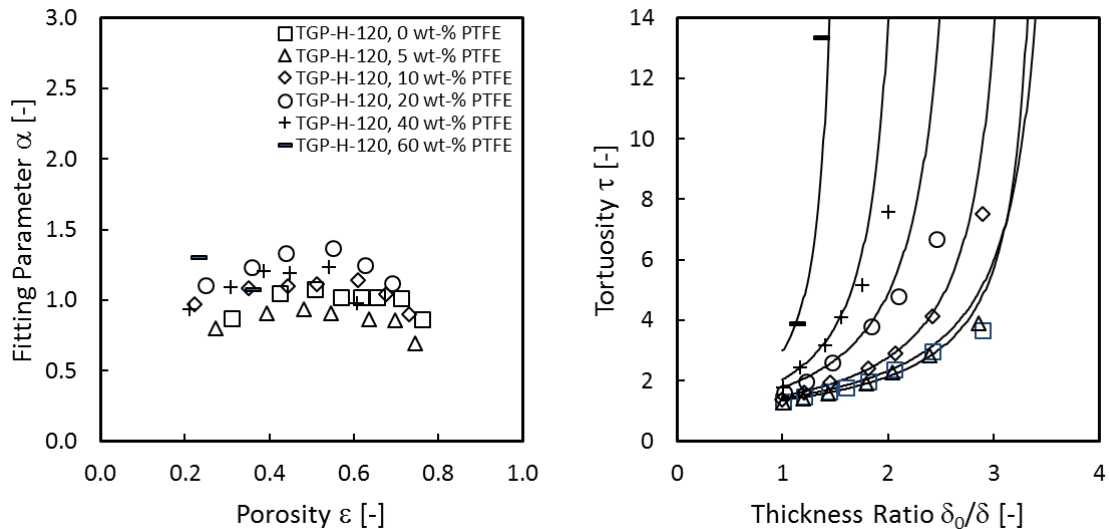


Figure 19: Fitted percolation model through measured tortuosities vs. thickness ratio (left) and determined α -values vs. compressed porosity (right) of untreated and treated TGP-H-120.

The idea of fiber breakage and morphological changes altering tortuosity can be explored further by fitting Eq. (17) to each point individually, which results in the distribution of α values shown in Figure 19(right). For the samples with low PTFE loadings (0-20 wt-%), α values rise slightly from the first to second compression points, then plateau until a compressed porosity of 40% is reached. After this porosity, α values begin to drop. The initial rise in α was possibly due to the surfaces of the sample becoming more tightly sealed against the wall of the holder as it was tightened. The plateau in the α values indicates that the sample morphology remained constant between points. The drop in α below compressed porosity of about 40% indicates that the structure was changing and it was indeed becoming less tortuous, suggesting cracks and breakage. The samples with higher PTFE loading (>20 wt-%) display the same trend but show less notable plateaus in α . The plateau values of α observed in Figure 19(right) correspond to the values required to obtain the full curve fits shown in Figure 19(left).

The overall picture of tortuosity as a function of compression then appears to be that samples generally maintain their structural integrity at low-to-mid range levels of compression, as indicated by relatively constant α values, but begin to deform fundamentally below compressed porosities of 40%. Plateau values of α (above 40% porosity) are approximately 1.0 (0.9-1.1) for low PTFE loading samples, and increase to 1.3-1.4 for higher PTFE samples. That these values are somewhat higher than the values of 0.6-0.8 values reported for simulations on idealized fiber structures [55], which is to be expected, given the additional material (i.e. binder and PTFE) found in the pore space of real materials. Thus, it can be recommended that for reasonable compressions (less than a thickness ratio of 2), similar to those experienced in assembled fuel cells, Eq. (17) correlates tortuosity with porosity in an acceptable manner using the α values obtained at low compression.

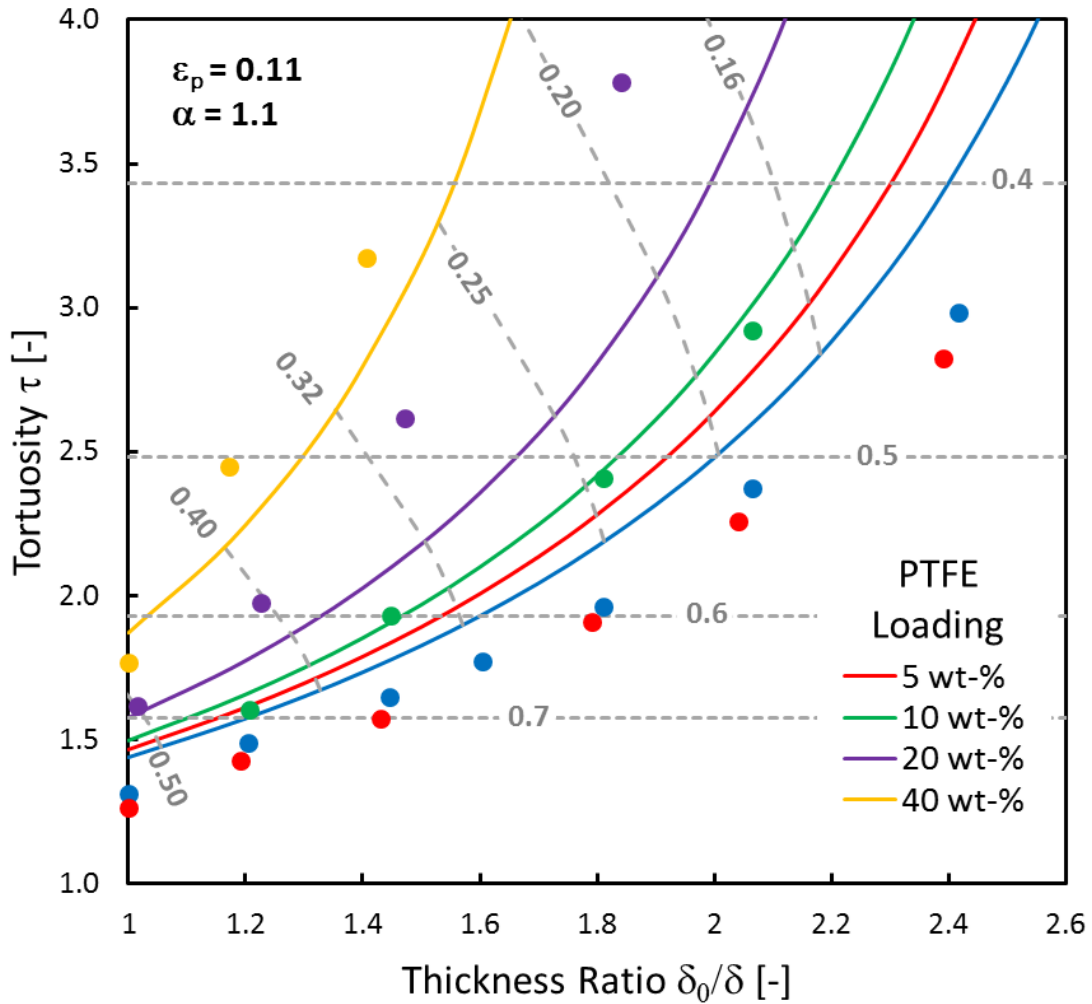


Figure 20: Predicted trends in tortuosity as a function of thickness ratio with PTFE loading as a parameter, indicated by the solid colored curves. The horizontal dashed lines are isolines of constant porosity, while the sloping dashed rules are isolines of constant normalized effective diffusivity. Experimental data points are included for comparison and color-coded according to PTFE loading.

It is noteworthy that the plateau values of α shown in Figure 19(right) are all quite similar (0.9-1.3) for the various different PTFE loadings. It is of interest to determine if a single α value lying in this range can reasonable predict τ values at a specified PTFE loadings and thickness ratios knowing only the properties of the virgin material (untreated and uncompressed). Lim and Wang [69] presented the following relationship for determining the porosity of a PTFE treated sample:

$$\varepsilon = \varepsilon_0 - \frac{w \rho_{GDL,0}}{1 - w \rho_{PTFE}} \quad \text{Eq. (18)}$$

where $\rho_{GDL,0}$ is the bulk density of an untreated GDL, ρ_{PTFE} is the density of PTFE, w is the mass fraction of PTFE in the sample, and ε_0 is the porosity of the untreated material. The applicability of Eq. (18) has recently been scrutinized [3], and found to hold so long as w is accurately known. The value of porosity given by this equation can then be combined with Eq. (13) in order to determine the compressed porosity at a specified thickness ratio. Finally, the compressed porosity can be used in Eq. (17) to obtain a tortuosity value. Figure 20 compares the results of this calculation using $\alpha = 1.1$ with the experimental data for TGP-H-120 at thickness ratios below 2.5. The fit of the lines to the data points is not as tight as in Figure 19(right), where unique values of α were used for each curve. Nonetheless, the model and the experimental data appear to be in fair agreement, especially considering that this figure is zoomed into a smaller range of thickness ratios. Tortuosity is over-predicted for low PTFE loadings and under-predicted for high loadings, since the chosen value of α corresponded to an intermediate PTFE loading (10%). The average difference between the model and data is 12%, with maximum deviation of 37% for the highest compression point of the highest PTFE loading sample. If the 3 worst fitting points are removed (belonging to the higher PTFE samples and at the highest thickness ratios) then the average deviation drops to 7% with a maximum of 15%. It seems that this simple model for estimating tortuosity of any material from easily known properties of the base material is quite acceptable, and could prove useful for any general modeling calculations where reasonable engineering estimates are required. Similar agreement was found with TGP-H-060 and TGP-H-090 up to 20 wt-% PTFE loading using $\alpha = 1.0$, and for Freudenberg H2315 with $\alpha = 0.8$. The SGL materials did not show a plateau in α values as seen Figure 19(right), so the described approach cannot be applied.

3.5. Conclusions

The in-plane effective diffusion coefficients of untreated and PTFE-treated Toray, SGL, and Freudenberg gas diffusion layers used in PEMFCs were experimentally measured as a

function of compression using a previously developed technique. Effective diffusivities were observed to decrease with higher compressions. For each type of material, the measured effective diffusivity values as a function of compressed porosity collapsed on top of each regardless of PTFE loading. Unexpectedly, effective diffusivities of Freudenberg H2315 were measured higher than Toray and SGL materials, with SGL GDLs exhibiting the least diffusive.

The presence of binder observed in the GDL proved to significantly impact the effective diffusivity. While SEM images displayed the porous nature of the binder used in SGL materials, Toray GDLs contained a much less porous and smoother binder. Freudenberg H2315 material appeared to have no visible binder. The porous binder in SGL materials was expected to contribute to the overall porosity but not to mass transport characteristics.

In order to differentiate the effects of PTFE loading and compression on tortuosity, tortuosity was plotted as a function of compressed thickness. By comparing samples at equal compressions, rather than equal porosity, it was possible to clearly show the impact of PTFE in isolation since carbon volume fraction was constant between data points. This analysis revealed the effect of PTFE increases tortuosity as well as decreases porosity. Though this tendency was slight at lower PTFE-loadings, the trend became quite strong for higher PTFE loading, and as the medium is compressed.

As a result of compression, the porous samples became more tortuous, however, at low compressed porosity, tortuosities did not approach infinity, and therefore a percolation threshold was not observed. This was attributed to damage of the fiber structure and introduction of cracks at increased compressions, and thus, effectively increasing the available transport paths for diffusion.

The determined tortuosities of treated and untreated TGP-H-120 samples were fitted with

a single-parameter percolation model with 0.11 defined as percolation threshold. The agreement between experimental data and model quite good at low and moderate compressions, however, increasingly large discrepancies were seen for higher compressions, as experimental data tended to fall below the predicted tortuosity. This behavior was attributed to damage to the fibrous structure caused by high compressions, leading to a cracked solid structure and the creation additional diffusive pathways. The range of α -values required to fit each sample was not too large, so an attempt was made to model all TGP-H-120 samples simultaneously with a single value of α . It was found that for low to moderate compressions and PTFE loadings, similar to those found in operating cells, a reasonable estimate for tortuosity was obtained that would be suitable for engineering and modeling calculations.

3.6. Acknowledgements

The funding provided by the Automotive Fuel Cell Cooperation (AFCC) and the Natural Sciences and Engineering Research Council (NSERC) of Canada is greatly appreciated. The authors also wish to thank SGL Group for donating GDL sample materials.

3.7. Appendix

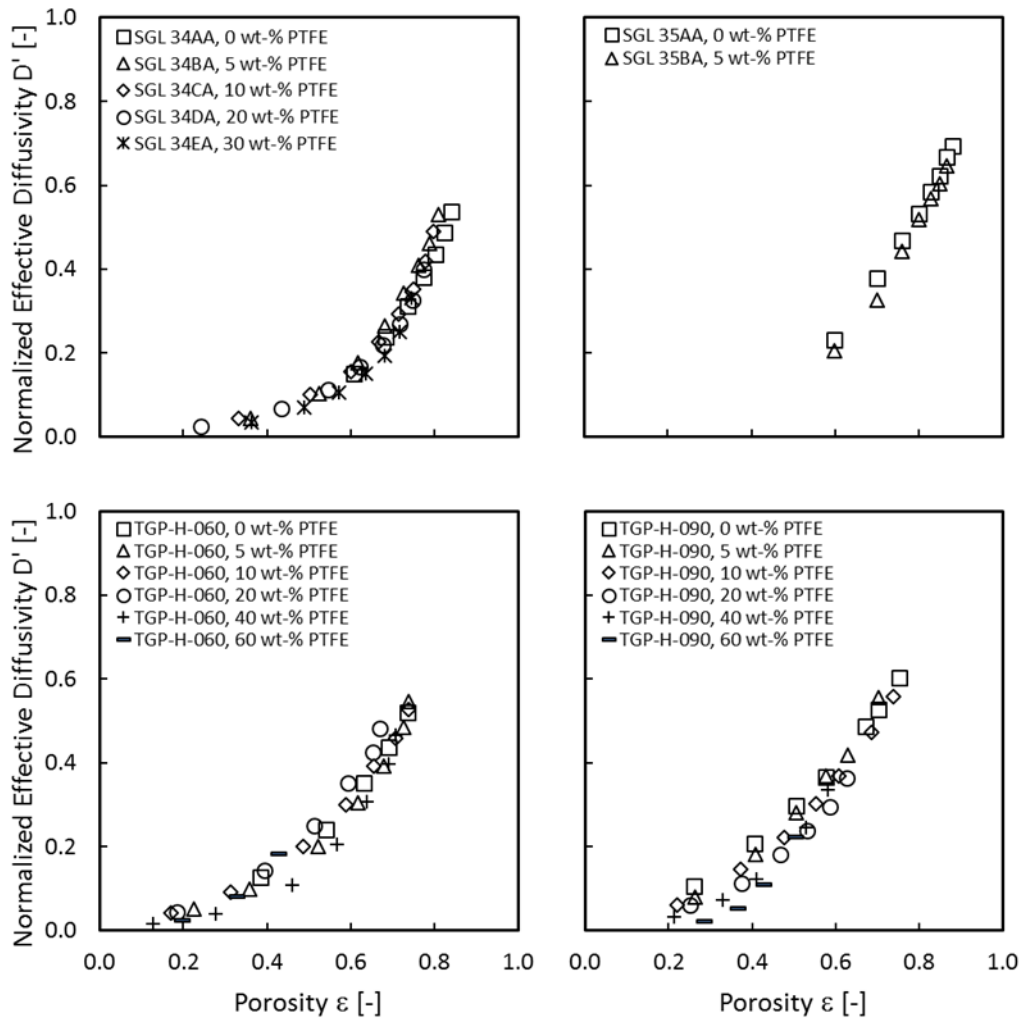


Figure 21: Normalized effective diffusivity D' vs. compressed porosity ϵ of untreated and treated SGL 34, SGL 35, TGP-H-060, and TGP-H-090.

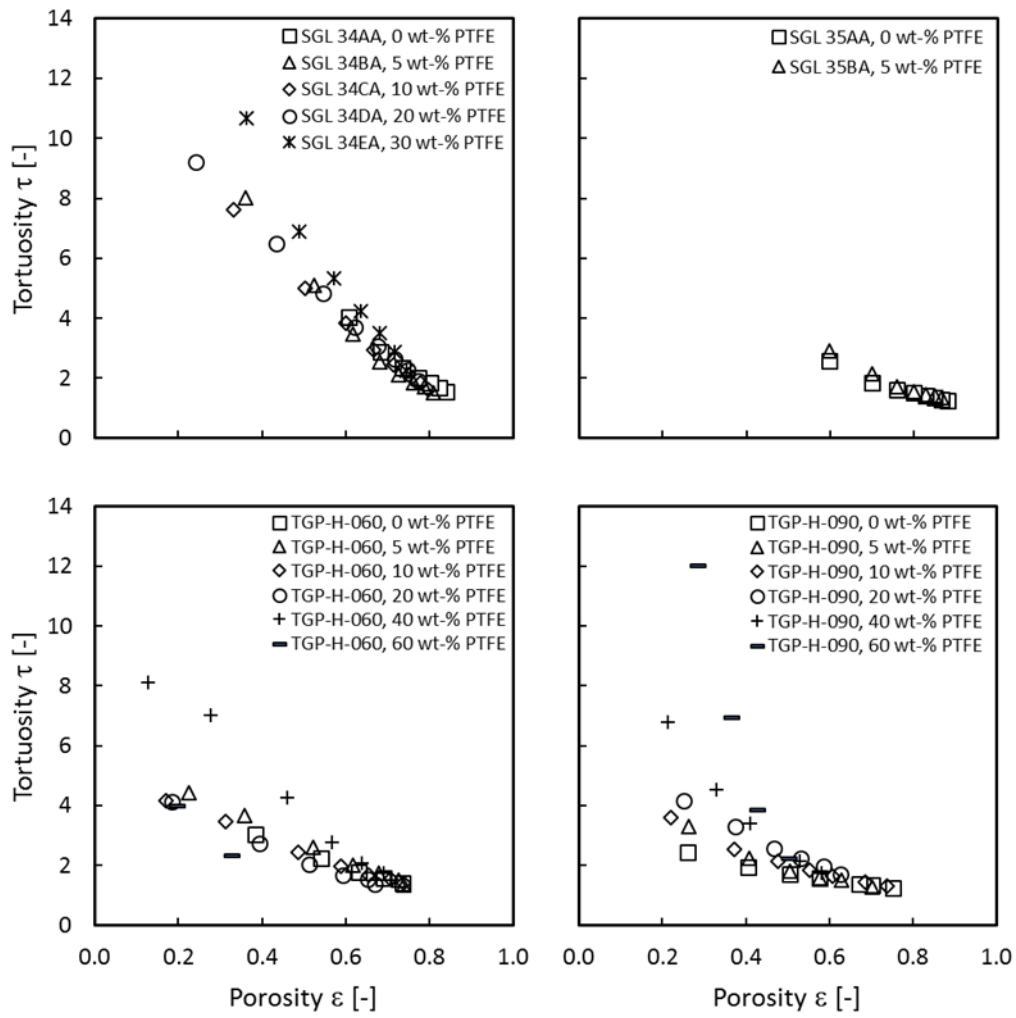


Figure 22: Tortuosity τ vs. compressed porosity ε of untreated and treated SGL 34, SGL 35, TGP-H-060, and TGP-H-090.

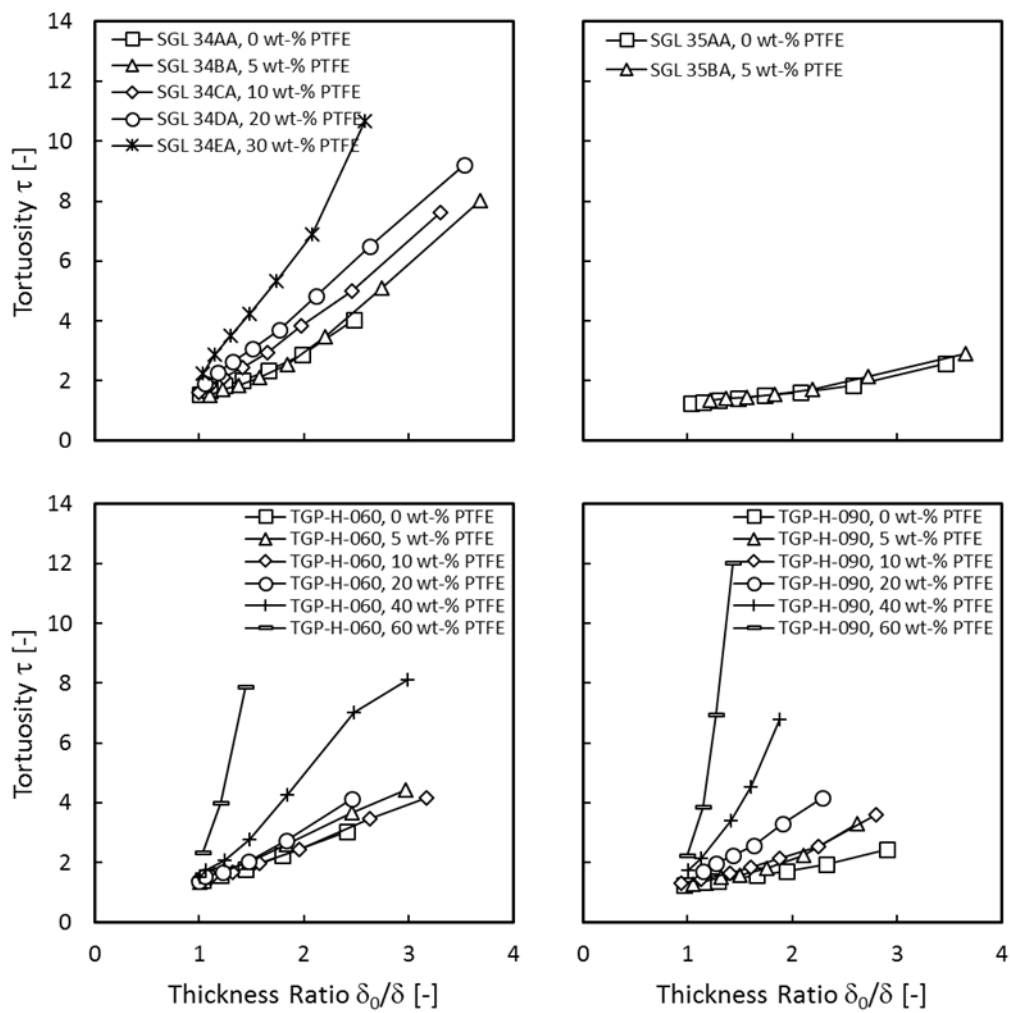


Figure 23: Tortuosity τ vs. thickness ratio δ_0/δ of untreated and treated SGL 25, SGL 35, TGP-H-060, and TGP-H-060.

Chapter 4: Final Conclusions & Recommendations

A straightforward and cost-effective experimental technique to measure the in-plane (IP) effective diffusivity of single layers of thin porous materials such as gas diffusion layers (GDLs) for PEMFCs was developed and validated. This method accurately reproduced the bulk diffusion coefficient of oxygen in nitrogen in various configurations, indicating the robustness of this approach. Using this method, the IP effective diffusion coefficients of untreated and PTFE-treated Toray, SGL, and Freudenberg gas diffusion layers used in PEMFCs were successfully measured as a function of compression. The following results can be summarized:

- Effective diffusivities were observed to decrease with higher compressions. For each type of material, the measured effective diffusivity values at a given compressed porosity collapsed on top of each, regardless of PTFE loading.
- As a result of compression, the porous samples became more tortuous, however, at very high compressions, tortuosities did not approach infinity, and therefore a percolation threshold was practically not observed. This was attributed to damage of the fiber structure and introduction of cracks at increased compressions.
- Tortuosity plotted as a function of compressed thickness revealed the effect of PTFE on effective diffusivity, as GDLs with PTFE addition had decreased initial porosity, while increasing tortuosity. This trend especially unfolds for higher teflonated GDLs as the medium is compressed.
- In addition to PTFE, the choice and amount of binder applied to the GDL significantly impact effective diffusivity. While SEM images displayed a brittle and porous nature of the binder used in SGL materials, Toray GDLs contained a much less porous and smoother binder. Freudenberg H2315 material appeared to have

no visible binder. The porous binder in SGL materials was expected to contribute to the overall porosity but not to mass transport characteristics.

- The calculated tortuosities of treated and untreated TGP-H-120 samples were fitted with a single-parameter percolation model. The agreement between experimental data and model was excellent at low and moderate compressions, however, major discrepancies were observed when the sample was compressed extensively. It was suggested that this behavior was due to the introduced damage to the fibrous structure as compressions increased.

The following recommendations to future works are made:

- Develop similar experimental technique to measure through-plane diffusivity and determine degree of anisotropy of GDLs.
- Measure effective diffusion coefficients in through-plane and in-plane direction as a function of relative humidity and saturation.
- Determine effect of a micro-porous layer on effective in-plane diffusivities.

References

- [1] R. Rashapov, F. Imami, and J. T. Gostick, "A method for measuring in-plane effective diffusivity in thin porous media," *International Journal of Heat and Mass Transfer*, vol. 85, pp. 367-374, 2015.
- [2] R. Rashapov and J. T. Gostick, "In-plane effective diffusivity in PEMFC gas diffusion layers," *Transport in Porous Media*, 2015, submitted.
- [3] R. R. Rashapov, J. Unno, and J. T. Gostick, "Characterization of PEMFC Gas Diffusion Layer Porosity," *Journal of The Electrochemical Society*, vol. 162, pp. F603-F612, January 1, 2015.
- [4] "2014 World Population Data Sheet," P. R. Bureau, Ed., ed. Washington, D.C., 2014.
- [5] "International Energy Statistics," U. S. E. I. Administration, Ed., ed. Washington, DC, 2014.
- [6] S. Chu and A. Majumdar, "Opportunities and challenges for a sustainable energy future," *Nature*, vol. 488, pp. 294-303, 2012.
- [7] M. K. Hubbert, *Nuclear energy and the fossil fuels* vol. 95: Shell Development Company, Exploration and Production Research Division Houston, TX, 1956.
- [8] M. K. Hubbert, "Survey of world energy resources," *Energy Sources Future*, p. 1, 1975.
- [9] P. De Almeida and P. D. Silva, "The peak of oil production—timings and market recognition," *Energy Policy*, vol. 37, pp. 1267-1276, 2009.
- [10] "United Nations Framework Convention on Climate Change", 1992.
- [11] B. G. Pollet, I. Staffell, and J. L. Shang, "Current status of hybrid, battery and fuel cell electric vehicles: From electrochemistry to market prospects," *Electrochimica Acta*, vol. 84, pp. 235-249, 2012.
- [12] B. Verspagen, "Mapping technological trajectories as patent citation networks: A study on the history of fuel cell research," *Advances in Complex Systems*, vol. 10, pp. 93-115, 2007.
- [13] C. F. Schönbein, "Beobachtungen über den bei der Elektrolyse des Wassers und dem Ausströmen der gewöhnlichen Elektrizität aus Spitzen sich entwickelnden Geruch," *Annalen der Physik*, vol. 126, pp. 616-635, 1840.

- [14] J. M. Andújar and F. Segura, "Fuel cells: History and updating. A walk along two centuries," *Renewable and Sustainable Energy Reviews*, vol. 13, pp. 2309-2322, 2009.
- [15] N. Zamel and X. Li, "Effective transport properties for polymer electrolyte membrane fuel cells – With a focus on the gas diffusion layer," *Progress in Energy and Combustion Science*, vol. 39, pp. 111-146, 2013.
- [16] J. T. Gostick, M. A. Ioannidis, M. W. Fowler, and M. D. Pritzker, "On the role of the microporous layer in PEMFC operation," *Electrochemistry Communications*, vol. 11, pp. 576-579, 2009.
- [17] E. N. Fuller, P. D. Schettler, and J. C. Giddings, "New method for prediction of binary gas-phase diffusion coefficients," *Industrial & Engineering Chemistry*, vol. 58, pp. 18-27, 1966.
- [18] M. B. Clennell, "Tortuosity: a guide through the maze," *Geological Society, London, Special Publications*, vol. 122, pp. 299-344, 1997.
- [19] N. Epstein, "On tortuosity and the tortuosity factor in flow and diffusion through porous media," *Chemical Engineering Science*, vol. 44, pp. 777-779, 1989.
- [20] B. Ghanbarian, A. G. Hunt, R. P. Ewing, and M. Sahimi, "Tortuosity in porous media: a critical review," *Soil Science Society of America Journal*, vol. 77, pp. 1461-1477, 2013.
- [21] L. Shen and Z. Chen, "Critical review of the impact of tortuosity on diffusion," *Chemical Engineering Science*, vol. 62, pp. 3748-3755, 2007.
- [22] R. Cortright, R. Davda, and J. Dumesic, "Hydrogen from catalytic reforming of biomass-derived hydrocarbons in liquid water," *Nature*, vol. 418, pp. 964-967, 2002.
- [23] A. L. Dicks, "Hydrogen generation from natural gas for the fuel cell systems of tomorrow," *Journal of Power Sources*, vol. 61, pp. 113-124, 1996.
- [24] F. Barbir, "PEM electrolysis for production of hydrogen from renewable energy sources," *Solar Energy*, vol. 78, pp. 661-669, 2005.
- [25] J. D. Holladay, J. Hu, D. L. King, and Y. Wang, "An overview of hydrogen production technologies," *Catalysis Today*, vol. 139, pp. 244-260, 2009.
- [26] D. L. G. G. Duleep, "Status and Prospects of the Global Automotive Fuel Cell Industry and Plans for Deployment of Fuel Cell Vehicles and Hydrogen Refueling Infrastructure," 2013.

- [27] V. Mehta and J. S. Cooper, "Review and analysis of PEM fuel cell design and manufacturing," *Journal of Power Sources*, vol. 114, pp. 32-53, 2003.
- [28] Y. Wang, K. S. Chen, J. Mishler, S. C. Cho, and X. C. Adroher, "A review of polymer electrolyte membrane fuel cells: technology, applications, and needs on fundamental research," *Applied Energy*, vol. 88, pp. 981-1007, 2011.
- [29] F. Barbir, *PEM fuel cells: Theory and Practice*: Academic Press, 2013.
- [30] W. Vielstich, *Handbook of Fuel Cells: Fundamentals, Technology, Applications, 4-Volume Set*, 2003.
- [31] L. M. Pant, S. K. Mitra, and M. Secanell, "Absolute permeability and Knudsen diffusivity measurements in PEMFC gas diffusion layers and micro porous layers," *Journal of Power Sources*, vol. 206, pp. 153-160, 2012.
- [32] J. Bear and Y. Corapcioglu, *Transport processes in porous media*: Kluwer Academic Publishers, 1991.
- [33] F. A. Dullien, *Porous media: fluid transport and pore structure*: Academic press, 1991.
- [34] D. Kramer, S. A. Freunberger, R. Flückiger, I. A. Schneider, A. Wokaun, F. N. Büchi, *et al.*, "Electrochemical diffusimetry of fuel cell gas diffusion layers," *Journal of Electroanalytical Chemistry*, vol. 612, pp. 63-77, 2008.
- [35] N. G. C. Astrath, J. Shen, D. Song, J. H. Rohling, F. B. G. Astrath, J. Zhou, *et al.*, "The Effect of Relative Humidity on Binary Gas Diffusion," *The Journal of Physical Chemistry B*, vol. 113, pp. 8369-8374, 2009/06/18, 2009.
- [36] J. P. Holman, *Experimental Methods for Engineers*: McGraw-Hill, 2001.
- [37] N. Zamel, N. G. C. Astrath, X. Li, J. Shen, J. Zhou, F. B. G. Astrath, *et al.*, "Experimental measurements of effective diffusion coefficient of oxygen–nitrogen mixture in PEM fuel cell diffusion media," *Chemical Engineering Science*, vol. 65, pp. 931-937, 2010.
- [38] C. Quick, D. Ritzinger, W. Lehnert, and C. Hartnig, "Characterization of water transport in gas diffusion media," *Journal of Power Sources*, vol. 190, pp. 110-120, 2009.
- [39] J. M. LaManna and S. G. Kandlikar, "Determination of effective water vapor diffusion coefficient in pemfc gas diffusion layers," *International Journal of Hydrogen Energy*, vol. 36, pp. 5021-5029, 2011.

- [40] D. R. Baker, C. Wieser, K. C. Neyerlin, and M. W. Murphy, "The Use of Limiting Current to Determine Transport Resistance in PEM Fuel Cells," *ECS Transactions*, vol. 3, pp. 989-999, October 20, 2006.
- [41] Y. Utaka, Y. Tasaki, S. Wang, T. Ishiji, and S. Uchikoshi, "Method of measuring oxygen diffusivity in microporous media," *International Journal of Heat and Mass Transfer*, vol. 52, pp. 3685-3692, 2009.
- [42] G. S. Hwang and A. Z. Weber, "Effective-Diffusivity Measurement of Partially-Saturated Fuel-Cell Gas-Diffusion Layers," *Journal of The Electrochemical Society*, vol. 159, pp. F683-F692, January 1, 2012.
- [43] D. R. Baker, D. A. Caulk, K. C. Neyerlin, and M. W. Murphy, "Measurement of Oxygen Transport Resistance in PEM Fuel Cells by Limiting Current Methods," *Journal of The Electrochemical Society*, vol. 156, pp. B991-B1003, September 1, 2009.
- [44] R. Flückiger, S. A. Freunberger, D. Kramer, A. Wokaun, G. G. Scherer, and F. N. Büchi, "Anisotropic, effective diffusivity of porous gas diffusion layer materials for PEFC," *Electrochimica Acta*, vol. 54, pp. 551-559, 2008.
- [45] I. Ocean Optics, "Neofox and NeoFox Sport Installation and Operation Manual," 2010.
- [46] J. Crank, *The mathematics of diffusion*: Oxford university press, 1979.
- [47] S. Yasuaki Ichikawa, A.P.S., *Transport Phenomena in Porous Media*: Springer, 2012.
- [48] M. Y. C. Jacob Bear, *Transport processes in porous media*: Kluwer Academic Publishers, 1991.
- [49] J. Delgado, "A simple experimental technique to measure tortuosity in packed beds," *The Canadian Journal of Chemical Engineering*, vol. 84, pp. 651-655, 2006.
- [50] J. T. Gostick, M. A. Ioannidis, M. W. Fowler, and M. D. Pritzker, "Pore network modeling of fibrous gas diffusion layers for polymer electrolyte membrane fuel cells," *Journal of Power Sources*, vol. 173, pp. 277-290, 2007.
- [51] Z. H. Fishman, J.; Bazylak, A., "Anisotropic Porosity Profiles of PEMFC GDLs," presented at the ASME 2010 8th International Conference on Fuel Cell Science, Engineering and Technology, Brooklyn, New York, USA, 2010.
- [52] B. Smitha, S. Sridhar, and A. Khan, "Solid polymer electrolyte membranes for fuel cell applications—a review," *Journal of Membrane Science*, vol. 259, pp. 10-26, 2005.

- [53] L. Cindrella, A. M. Kannan, J. F. Lin, K. Saminathan, Y. Ho, C. W. Lin, *et al.*, "Gas diffusion layer for proton exchange membrane fuel cells—A review," *Journal of Power Sources*, vol. 194, pp. 146-160, 2009.
- [54] D. A. G. Bruggeman, "Berechnung verschiedener physikalischer Konstanten von heterogenen Substanzen. I. Dielektrizitätskonstanten und Leitfähigkeiten der Mischkörper aus isotropen Substanzen," *Annalen der Physik*, vol. 416, pp. 636-664, 1935.
- [55] M. M. Tomadakis and S. V. Sotirchos, "Ordinary, transition, and Knudsen regime diffusion in random capillary structures," *Chemical Engineering Science*, vol. 48, pp. 3323-3333, 1993.
- [56] M. M. Tomadakis and S. V. Sotirchos, "Effective diffusivities and conductivities of random dispersions of nonoverlapping and partially overlapping unidirectional fibers," *The Journal of chemical physics*, vol. 99, pp. 9820-9827, 1993.
- [57] J. G. Pharoah, K. Karan, and W. Sun, "On effective transport coefficients in PEM fuel cell electrodes: Anisotropy of the porous transport layers," *Journal of Power Sources*, vol. 161, pp. 214-224, 2006.
- [58] N. Astrath, J. Shen, F. Astrath, J. Zhou, C. Huang, X. Yuan, *et al.*, "Note: Determination of effective gas diffusion coefficients of stainless steel films with differently shaped holes using a Loschmidt diffusion cell," *Review of Scientific Instruments*, vol. 81, p. 046104, 2010.
- [59] Y. Utaka, D. Iwasaki, Y. Tasaki, and S. Wang, "Measurement of effective oxygen diffusivity in microporous media containing moisture," *Heat Transfer—Asian Research*, vol. 39, pp. 262-276, 2010.
- [60] Z. Fishman and A. Bazylak, "Heterogeneous Through-Plane Distributions of Tortuosity, Effective Diffusivity, and Permeability for PEMFC GDLs," *Journal of The Electrochemical Society*, vol. 158, pp. B247-B252, February 1, 2011.
- [61] B. Ramos-Alvarado, J. D. Sole, A. Hernandez-Guerrero, and M. W. Ellis, "Experimental characterization of the water transport properties of PEM fuel cells diffusion media," *Journal of Power Sources*, vol. 218, pp. 221-232, 2012.
- [62] A. D. Santamaria, P. K. Das, J. C. MacDonald, and A. Z. Weber, "Liquid-Water Interactions with Gas-Diffusion-Layer Surfaces," *Journal of The Electrochemical Society*, vol. 161, pp. F1184-F1193, January 1, 2014.
- [63] D. Shou, J. Fan, and F. Ding, "Effective diffusivity of gas diffusion layer in proton exchange membrane fuel cells," *Journal of Power Sources*, vol. 225, pp. 179-186, 2013.

- [64] P. K. Das, X. Li, and Z.-S. Liu, "Effective transport coefficients in PEM fuel cell catalyst and gas diffusion layers: Beyond Bruggeman approximation," *Applied Energy*, vol. 87, pp. 2785-2796, 2010.
- [65] Z. Hashin and S. Shtrikman, "A variational approach to the theory of the effective magnetic permeability of multiphase materials," *Journal of applied Physics*, vol. 33, pp. 3125-3131, 1962.
- [66] G. H. Neale and W. K. Nader, "Prediction of transport processes within porous media: diffusive flow processes within an homogeneous swarm of spherical particles," *AIChE Journal*, vol. 19, pp. 112-119, 1973.
- [67] N. Zamel, X. Li, and J. Shen, "Correlation for the effective gas diffusion coefficient in carbon paper diffusion media," *Energy & Fuels*, vol. 23, pp. 6070-6078, 2009.
- [68] M. Isichenko, "Percolation, statistical topography, and transport in random media," *Reviews of modern physics*, vol. 64, p. 961, 1992.
- [69] C. Lim and C. Wang, "Effects of hydrophobic polymer content in GDL on power performance of a PEM fuel cell," *Electrochimica Acta*, vol. 49, pp. 4149-4156, 2004.